## General Disclaimer

## One or more of the Following Statements may affect this Document

- This document has been reproduced from the best copy furnished by the organizational source. It is being released in the interest of making available as much information as possible.

- This document may contain data, which exceeds the sheet parameters. It was furnished in this condition by the organizational source and is the best copy available.

- This document may contain tone-on-tone or color graphs, charts and/or pictures, which have been reproduced in black and white.

- This document is paginated as submitted by the original source.

- Portions of this document are not fully legible due to the historical nature of some of the material. However, it is the best reproduction available from the original submission.

APOLLO SPACECRAFT SYSTEMS ANALYSIS PROGRAM

TECHNICAL REPORT

TASK E-34E

# LM LANDING RADAR PERFORMANCE OVER ROUGH TERRAIN

NAS 9-8166

14 NOVEMBER 1969

Prepared For

NATIONAL AERONAUTICS AND SPACE ADMINISTRATION
MANNED SPACECRAFT CENTER
HOUSTON, TEXAS

Prepared By

Communications and Sensor Systems Department
Electronics Systems Laboratory



TRW SYSTEMS GROUP

NASA CR 112017

11176-H397-R0-00

# APOLLO SPACECRAFT SYSTEMS ANALYSIS PROGRAM
# TECHNICAL REPORT
# TASK E-34E

# LM LANDING RADAR PERFORMANCE OVER ROUGH TERRAIN

NAS 9-8166

14 NOVEMBER 1969

Prepared For

NATIONAL AERONAUTICS AND SPACE ADMINISTRATION
MANNED SPACECRAFT CENTER
HOUSTON, TEXAS

Prepared By: J. N. Sappington
M. D. Zuteck

Approved by: Charles E. Blakely
C. E. Blakely, Manager
Task E-34E

Approved by:
J. DeVillier, Manager Communications
and Sensor Systems Department

CONTENTS

## ILLUSTRATIONS

ILLUSTRATIONS - (Continued)

## TABLES

## 1.0 INTRODUCTION

The purpose of this report is to show the effects of rough terrain on the Landing Radar performance by using PEARL Project Flight Test data. The PEARL Project was conducted in 1968 at White Sands Missle Range where the Landing Radar was flown over both smooth and rough terrain in both the SH-3A Test Helicopter and the T-33 Test Aircraft. During each flight test the Landing Radar provided component velocity ($V_x$, $V_y$, and $V_z$) and slant range measurements which are used in this report. A cinetheodolite tracking system was also employed to provide a reference standard for each measured Landing Radar parameter. Vector velocity magnitudes were derived from these radar and cinetheodolite data as an auxiliary parameter.

In this report portions of test data were considered from five flight tests of the PEARL Project. Specifically, these flight tests consist of three flights over Little Burro Peak, LR-58E using the SH-3A Helicopter, LR-74E using the T-33 Aircraft, and LR-77E using the T-33 Aircraft; two flights were over smooth terrain, LR-60J using the SH-3A Helicopter and LR-73F using the T-33 Aircraft. References 1, 2, 3, 4, and 8 contain these data.

Landing Radar data are plotted and appear in Figures 1 through 10 and 13 through 22. Cinetheodolite - Landing Radar difference data are plotted and appear in Figures 11, 12, 23, and 24.

It was determined that no direct comparison or correlation could be made of data from flights over rough and smooth terrain. Basic reasons were as follows. Sufficient data were not available. Some flights were level, and some showed variations in their flight paths. Different scale factor modes were used within the same pass of a single flight. Therefore, the major portions of analysis utilize LR-58E data since this flight produced the best data. Computer-fitted curves were obtained for zero through the ninth-degree polynomials. Bias and residual data, extracted from this computer information, appear in Figures 25 through 30.

Tracker lag was investigated as a possible cause of the observed slant range errors over rough terrain. A simplified model of the tracker based on measured data was used to estimate the effect of tracker lag on

slant range accuracy. The predictions of this model are compared with the measured data for both a T-33 Aircraft pass (Figure 36) and for a SH-3A Helicopter pass (Figure 37). Agreement between measured and estimated errors was found to be poor.

In Section 8 it is shown that significant velocity errors as well as range errors can be generated by some terrain types. It is also concluded that Little Burro Peak was sloped such that large range errors would be generated; however, only small perturbations would be experienced in the velocity measurements.

## 2.0 LANDING RADAR FLIGHTS LR-58E and LR-60J

### 2.1 FLIGHT DESCRIPTION

Flight LR-58E was performed over Little Burro Peak using a SH-3A Test Helicopter flying four straight and level passes at 8300 feet mean sea level (MSL). These passes consisted of:

Pass 1 at 60 knots on heading NW to SE
Pass 2 at 60 knots on heading SE to NW
Pass 3 at 60 knots on heading NW to SE
Pass 4 at 60 knots on heading SE to NW

Flight LR-60J was performed over smooth terrain using a SH-3A Test Helicopter flying seven descending passes beginning at 3000 feet above ground level (AGL) and at an initial forward speed of 43.5 $\pm$3 knots.

### 2.2 LANDING RADAR DATA

Pass 2 of LR-58E and pass 7 of LR-60J were used originally for rough terrain versus smooth terrain data comparisons. The Landing Radar data for both passes were plotted and are included in Figures 1 through 10. These data consist of slant range, component velocities ($V_x$, $V_y$, and $V_z$), and the magnitude of the vector velocity. Additionally, Figures 5 and 10 show a comparison of the magnitude of vector velocity for the Landing Radar and cinetheodolite.

For all data plots the Landing Radar and/or the cinetheodolite mean value averaged over five eighty-millisecond samples was used. The five eighty-millisecond samples are grouped around points separated by two-second intervals along the time scale.

### 2.3 CINETHEODOLITE - LANDING RADAR DIFFERENCE DATA

Pass 2 of LR-58E and pass 7 of LR-60J were used originally for rough terrain versus smooth terrain data comparisons. The cinetheodolite and Landing Radar difference data for both passes were plotted and are included in Figures 11 and 12. These difference data consist of slant range, component velocities ($V_x$, $V_y$, and $V_z$), and the magnitude of the vector velocity. A terrain profile of Little Burro Peak, derived from the cinetheodolite slant range, was also plotted and is included in Figure 11.

For all data plots, except the terrain profile, the differences in the Landing Radar and the cinetheodolite mean value averaged over five eighty-millisecond samples were used. The five eighty-millisecond samples are grouped around points separated by two-second intervals along the time scale. The specification values were taken from LSP-470-2D, "Master End Item Specification," as given in Table 1 and Reference 5. The specification limits as depicted by solid lines on the plots are calculated from the cinetheodolite vector velocity and slant range.

# 3.0 LANDING RADAR FLIGHTS LR-77E AND LR-73F

## 3.1 FLIGHT DESCRIPTION

Flight LR-77E was performed over Little Burro Peak using a T-33 Test Aircraft flying three straight and level passes at 8500 feet MSL. These passes consisted of:

Pass 1 at 300 knots on heading SE to NW
Pass 2 at 300 knots on heading NW to SE
Pass 3 at 400 knots on heading SE to NW

Flight LR-73F was performed over smooth terrain using a T-33 Test Aircraft flying seven south to north passes beginning level and ending in a climb.

Pass 1 at 200 knots at 3000 ft AGL
Pass 2 at 200 knots at 3000 ft AGL
Pass 3 at 200 knots at 3000 ft AGL
Pass 4 at 400 knots at 5000 ft AGL
Pass 5 at 400 knots at 5000 ft AGL
Pass 6 at 400 knots at 5000 ft AGL
Pass 7 at 200 knots at 3000 ft AGL

## 3.2 LANDING RADAR DATA

Pass 3 of LR-77E and pass 1 of LR-73F were used originally for rough terrain versus smooth terrain data comparisons. The Landing Radar data for both passes were plotted and are included in Figures 13 through 22. These data consist of slant range, component velocities ($V_x$, $V_y$, and $V_z$), and the magnitude of the vector velocity. Additionally, Figures 17 and 22 show a comparison of the magnitude of vector velocity for the Landing Radar and cinetheodolite.

For all data plots the Landing Radar and/or the cinetheodolite mean value averaged over five eighty-millisecond samples was used. The five eighty-millisecond samples are grouped around points separated by two-second intervals along the time scale.

## 3.3 CINETHEODOLITE - LANDING RADAR DIFFERENCE DATA

Pass 3 of LR-77E and pass 1 of LR-73F were used originally for rough terrain versus smooth terrain data comparisons. The cinetheodolite and Landing Radar difference data for both passes were plotted and are included in Figures 23 and 24. These difference data consist of slant range, component velocities ($V_x$, $V_y$, and $V_z$), and the magnitude of the vector velocity. A terrain profile of Little Burro Peak, derived from the cinetheodolite slant range, was also plotted and is included in Figure 23.

For all data plots, except the terrain profile, the differences in the Landing Radar and the cinetheodolite mean value averaged over five eighty-millisecond samples were used. The five eighty-millisecond samples are grouped around points separated by two-second intervals along the time scale. The specification values were taken from LSP-470-2D, "Master End Item Specification", as given in Table 1 and Reference 5. The specification limits as depicted by solid lines on the plots are calculated from the cinetheodolite vector velocity and slant range.

# 4.0 LANDING RADAR FLIGHT LR-74E

## 4.1 FLIGHT DESCRIPTION

Flight LR-74E was performed over Little Burro Peak using a T-33 Test Aircraft flying five straight and level passes at 8500 feet MSL. These passes consisted of:

Pass 1 at 400 knots on heading NW to SE
Pass 2 at 400 knots on heading SE to NW
Pass 3 at 300 knots on heading NW to SE
Pass 4 at 300 knots on heading SE to NW
Pass 5 at 300 knots on heading NW to SE

## 4.2 FLIGHT DATA

Since Flight LR-74E and LR-77E were performed under very similar conditions, only LR-77E data were used for this analysis.

## 5.0 CINETHEODOLITE DATA

During each Landing Radar test a cinetheodolite tracking system was used as a reference standard for each measured Landing Radar parameter. The cinetheodolite tracking system is an N-station network of cameras which measures azimuth and elevation angles of the aircraft. After the azimuth and elevation angles were corrected for atmospheric refraction and systematic instrumentation errors, an N-station least-squares solution was used to compute the expected position of the aircraft. The computed position was determined at that point for which the sum of the squares of the angular difference between the expected position and observed position was a minimum. Each component velocity was obtained by evaluating the first derivative of the second-degree least squares curve fitted to N consecutive position points having their midpoint at the position of desired velocity.

In many instances cinetheodolite and Landing Radar component velocity ($V_x$, $V_y$, and $V_z$) values vary widely. This difference appears to have been generated during cinetheodolite data manipulations. A striking example of this discrepancy is given in Reference 1 for Pass 2 of LR-58E. The cinetheodolite vector velocity magnitude, which is not affected by this discrepancy, was used for raw data plots and the full computer analysis.

In all cinetheodolite and Landing Radar data comparisons, with few minor exceptions, the cinetheodolite data are much smoother than the Landing Radar data. This fact is verified by Figures 5, 10, 17, and 22 for cinetheodolite versus Landing Radar vector velocity magnitude for both smooth and rough terrain.

# 6.0 ANALYSIS OF DATA

## 6.1 DATA CONSIDERED

Originally, four test flights were investigated to provide data for this comparative analysis. The two flights over Little Burro Peak, LR-58E and LR-77E, and the two flights over smooth terrain, LR-60J and LR-73F, were chosen for analysis. Figures 12 and 24 indicate that cinetheodolite-Landing Radar difference data are within the specifications of Reference 5 when over smooth terrain. Figure 11 indicates that a major portion of the cinetheodolite-Landing Radar difference data fall outside the specifications of Reference 5 when over rough terrain. It was found, however, that no direct comparison or correlation could be made of data from flights over rough and smooth terrain because of basic differences in the flights as given in Sections 2 and 3. For example, different aircraft velocities, level versus variations in flight paths, and different scale factor modes were used in the flights over Little Burro Peak and over smooth terrain. Therefore, the data from LR-60J and LR-73F were discarded since a valid comparison with data over rough terrain could not be made.

From the two remaining flights, LR-58E and LR-77E, it was discovered that as both the SH-3A Helicopter and the T-33 Aircraft passed over the roughest portions of Little Burro Peak that the Landing Radar was operating in the low scale factor mode. As specified in Reference 5, the Landing Radar switched into the low scale factor at approximately 2500 feet slant range and switched out of it at approximately 3100 feet slant range.

Also, because of its higher velocity, the T-33 aircraft was over the roughest portions of Little Burro Peak for a time interval of a few seconds as compared to a much longer time for the SH-3A Helicopter. This aspect is verified by the terrain profile of Figures 11 and 23. Because of the limited number of data points during the low scale factor mode and high scale factor mode for the T-33 over Little Burro Peak, it was concluded that a statistical analysis would not be valid for data taken from LR-77E.

Therefore, the major portions of analysis utilize data from Pass 2 of LR-58E as given in Reference 1. As stated in Section 5, only the vector velocity magnitude was used for the complete analysis. The vector velocity difference given in Reference 1 is not a true vector difference since it considers only magnitude instead of both magnitude and direction.

Vector velocity difference as given by Computing and Software, Inc. was calculated by:

$$\Delta V = |\vec{V}_R| - |\vec{V}_C| \quad .$$

where:

$V_R$ - Radar vector velocity

$V_C$ - Cinetheodolite vector velocity

$\Delta V$ - Vector velocity difference

To use the term, vector velocity, is somewhat of a misnomer. It would be more properly called a difference of vector velocity magnitude.

The desired quantity, vector velocity difference, should be defined as:

$$|\Delta\vec{V}| = |\vec{V}_R - \vec{V}_C| \quad .$$

This difference, $\vec{V}_R - \vec{V}_C$, is a vectorial quantity since both magnitude and direction are considered in the operation.

## 6.2 COMPUTER ANALYSIS OF LR-58E DATA

The mathematical model used for computer-fitted curves is the same as the one utilized in Reference 6 and as modified by Reference 7. Data from pass 2 of LR-58E with the following qualifications were analyzed:

1. Only the magnitude of vector velocity, not both magnitude and direction, was considered for the complete analysis.

2. A portion of the pass (130 seconds to 216 seconds) was used as data taken over rough terrain.

3. A portion of the pass (272 seconds to 360 seconds) was used as data taken over smooth terrain.

4. Rough terrain data (130 seconds to 216 seconds) were in the low scale factor mode.

5. Smooth terrain data (272 seconds to 360 seconds) were not in the low scale factor mode.

The vector velocity magnitude input data to the computer for both smooth and rough terrain and for both the cinetheodolite and Landing Radar are compared by graphical representation in Figures 25 and 26. Except for a few isolated cases, the vector velocity magnitude for both smooth and rough terrain for the cinetheodolite fluctuates much less than that for the Landing Radar.

A computer statistical analysis was performed in which zero through ninth-degree computer-fitted curves were obtained for the best polynomial fit for smooth and rough terrain vector velocity magnitudes for both the cinetheodolite and Landing Radar. For third-degree Landing Radar curve fits the variance about the mean was 7.88 $ft^2/sec^2$ for rough terrain and 2.91 $ft^2/sec^2$ for smooth terrain. For third-degree cinetheodolite curve fits the variance about the mean was 17.7 $ft^2/sec^2$ for rough terrain and 2.2 $ft^2/sec^2$ for smooth terrain. The wide scatter about the mean for cinetheodolite rough terrain data is influenced by the unexplained fluctuations of the cinetheodolite data as indicated in Figure 26 (136 seconds to 152 seconds). Third-degree mean bias was 0.95 ft/sec for smooth terrain data and 1.23 ft/sec for rough terrain data.

The following computer-fitted information was hand plotted.

1. Third-degree polynomials, as given in Figures 27 and 28, indicate the bias (the Landing Radar polynomial minus the cinetheodolite polynomial).

2. Third-degree residuals, as given in Figures 29 and 30, were obtained by subtracting the third-degree polynomial value from the actual input value.

Except for the unexplained cinetheodolite fluctuations, Figures 27 and 28 indicate no appreciable difference in third-degree bias for vector velocity magnitude for smooth and rough terrain. Except for the unexplained cinetheodolite fluctuations, Figures 29 and 30 indicate that third-degree residuals for both smooth and rough terrain for the Landing Radar vector velocity magnitude data versus polynomial fit appear to follow the same pattern as those for the cinetheodolite vector velocity magnitude data versus its polynomial fit.

# 7.0 RANGE TRACKER LAG MODEL

## 7.1 DISCUSSION

Pass 1 of LR-77E is typical of the flight test data for the passes over Little Burro Peak. This flight was a T-33 jet aircraft flying a straight and level course at 8,500 feet mean sea level. The aircraft speed was 300 knots and the direction of the pass was from southeast to northwest along a 10 mile course.

Figure 31 is a reconstruction of the peak profile from the cine data. Figure 32 is a plot of the radar range errors as a function of time. The maximum error of the cine system and the radar specification errors combined is also plotted on this figure. The data employed in generating the figure are presented in Table 2.

It is obvious that the slant range errors are much larger than can be attributed to the range instrumentation system. An examination of the peak profile and the resulting error curve suggests that a dynamic lag error is being experienced. This section of the report presents the results of a tracker lag analysis and a comparison of the measured and calculated errors.

## 7.2 DEVELOPMENT OF A TRACKER FREQUENCY ERROR EQUATION

The landing radar frequency tracker may be described as a servo system which exhibits a dynamic lag plus a transient type error when subjected to a changing frequency spectrum. The rate of pull-in is related to the frequency discriminator and the closed loop gain.

An exact mathematical analysis of such a system is extremely complicated. However, a relatively simple model can be constructed from measured data which can be used to estimate the tracker behavior under transient conditions.

A simplified model was constructed as follows. An estimate of the tracker pull-in constant for signals well outside the discriminator-bandpass-filter characteristics was obtained from the slope of the curves in Figures 33 and 34. These data were presented by Ryan Aeronautical at the Ryan Landing Radar Technical meeting of 10 April 1968. They were also included in the meeting report. (Reference 9)

A good estimate of the pull-in rate is $17 \times 10^3$ cycles/second squared until the frequency difference is approximately 1200 cycles. This is illustrated in Figure 35. If a linear slope pull-in is assumed from 1200 cycles to zero frequency then the characteristic can be modelled as shown in Figure 35. The resulting differential equation for the system is

$$\frac{d\, f_t}{dt} = k\left( f_o(t) - f_t \right)$$

where

$$k = \frac{17 \times 10^3 \ \text{cycles/sec}^2}{1.2 \times 10^3 \ \text{cycles/sec}} = 14.2/\text{sec}$$

$f_t$ = Tracker frequency

$f_o(t)$ = Input signal frequency as a function of time

Assuming a linear frequency sweep for the input signal $f_o(t)$, the equation becomes

$$\frac{d\, f_t}{dt} = 14.2\ (At - f_t)$$

or in Laplace Transform form

$$sF(s) - F(o_+) = 14.2\, \frac{A}{s^2} - 14.2\, F(s)$$

and

$$F(s) = \frac{F(0_+)}{s + 14.2} + \frac{14.2\, A}{s^2(s + 14.2)}$$

$$f(t) = \left(F(o_+) + \frac{A}{14.2}\right) e^{-14.2t} + At - \frac{A}{14.2}$$

or

$$\text{Slant Range Error} = \frac{f(t) - At}{c} = \frac{1}{c}\left(F(o_+) + \frac{A}{14.2}\right)e^{-14.2t} - \frac{A}{14.2\ c}$$

where c is the factor relating frequency to distance.

$$(\text{freq.}) = c(\text{dist.})$$

Assuming that the velocity vector is at an angle $\phi$ with respect to the surface (this produces the linear frequency sweep assumed), the equation may be rewritten with

$$\frac{At}{c} = v \sin\phi\ t$$

or

$$A = c\ v \sin\phi$$

thus

$$\text{Slant Range Error} = \left(d(o_+) + \frac{v \sin\phi}{14.2}\right)e^{-14.2t} - \frac{v \sin\phi}{14.2}$$

This equation expresses the range error in terms of spacecraft velocity and angle of the velocity with respect to the surface.

## 7.3 NUMERICAL RESULTS

The above equation cannot be applied directly to the Little Burro Peak data because of the very long time interval between data samples (2 seconds). For comparison with these data it must be arbitrarily assumed that the transient term has decayed to zero and that the ground slope does not change over a two second interval. Introducing this restriction, the steady state lag can be calculated on a simplified basis.

$$\text{Slant Range Error} = \frac{v \sin\phi}{14.2} = \frac{1}{14.2} \overline{\frac{d(SR)}{dt}}$$

where slant range error is now given in terms of aircraft velocity and terrain slope, or alternately in terms of the average rate of change of slant range over the 2 second interval, $\overline{\frac{d(SR)}{dt}}$. Evaluation of this average derivative from cine slant range data yields the slant range error estimate shown in Figure 36. Figure 36 also shows measured slant range residuals and combined 3σ specification for comparison.

In order to further test the tracker lag hypothesis a similar estimate was made for pass 2 of flight LR-58E. In this flight the aircraft was an SH-3A helicopter and the helicopter velocity was 60 knots, which is 20% of that of the T-33. Examination of the simplified expression for slant range error due to tracker lag shows that a linear dependence of error on aircraft velocity is expected for similar terrain. Figure 37 shows the actual radar-cine residuals for pass 2 of flight LR-58E. Also shown is the error estimate based on tracker lag and the combined 3σ specification. The strong (5 to 1) dependence on aircraft velocity is not observed in the actual data. Table 3 gives the data on which the curves are based.

Frequency tracker lag does not appear to be the cause of the observed slant range errors over rough terrain. Slant range errors predicted on the basis of a simplified tracker model are too small to account for the observed errors. In addition, the velocity dependence of the errors which would be expected in the case of dynamic lag generated errors is not observed.

## 8.0 ADDITIONAL ROUGH TERRAIN EFFORT

The effect of rough terrain on landing radar performance is currently being investigated by math modeling the doppler power return spectrum as a function of terrain profile. The method is based on an extention of work done earlier regarding terrain modeling (References 10 and 11). At present a computer simulation is being employed to examine selected profiles chosen to approximate worst case conditions. Initial test cases have shown that it is possible to alter the return power spectrum quite significantly by proper terrain profile choice.

An example of such a return power spectrum is given in Figure 38. The terrain profile chosen in this instance was a two-level plane with a ramp joining the two levels. The slope of the ramp was chosen so that the ramp face would be perpendicular to the incident beam direction. This choice emphasizes the return from the ramp relative to the adjoining plane due to the higher reflectivity for normal incidence. The sharp rise and large peak in the return spectrum of Figure 38 are due to reflection from the ramp. Assuming that the frequency tracker responds to peak power, it is clear that the appearance of this reflection produced peak will cause a significant error in the tracker output frequency. The corresponding LR beam velocity would consequently be in error.

This example indicates that the existence of normal incidence reflecting areas within a velocity beam coverage pattern can produce significant LR velocity errors. It is to be noted that flights directly over a peak are unlikely to produce this situation since the predominant slope in that case would be away from the velocity beams, which are angled off to either side. Thus, the PEARL flights over Little Burro Peak leave much to be desired in terms of evaluating LR velocity errors. A better test of worst case velocity errors would be obtained by flying to one side of the peak, or along a ridge or valley. Since the altimeter beam is not angled off to one side, it would be more likely to view normal incidence reflecting areas within its pattern for a flight over a peak. For that reason it would be expected that the PEARL flights over Little Burro Peak more nearly provide a worst case condition for the altimeter beam than for the velocity beams.

It is planned to further generalize the computer simulation so that the return spectra for all three radar velocity beams can be obtained for a given surface profile. This would allow computation of the radar measured velocities. Comparison of these with the input spacecraft velocities would give simulated radar errors as a function of terrain profile. This capability would then be incorporated into the earlier radar simulation program LRTRW1. Extention of the computer model to include the return spectrum and errors for the altimeter beam as a function of terrain profile is also planned.

## 9.0 CONCLUSIONS

Based on the results presented in this report and on other studies that are currently in progress, the following conclusions have been reached.

1. Valid comparisons of data between different flights over smooth and rough terrain cannot be made.

2. Sufficient data are not available for valid statistical comparisons. Even those data in LR-58E for the component velocities ($V_x$, $V_y$, and $V_z$) are insufficient for a statistical analysis.

3. Vector velocity difference data do not indicate the vectorial difference since use was made of only the magnitude, not both magnitude and direction. Therefore, difference values do not give the true vector error information.

4. Only one rough terrain feature is available for comparative purposes.

5. The cinetheodolite-Landing Radar difference data depicted in Figures 11 and 23 indicate that a major portion of the slant range data is outside the specification limits of Reference 5 when both the T-33 Aircraft and SH-3A Helicopter are over the roughest portions of Little Burro Peak. Corresponding data are within specification limits when over the smoothest portions of Little Burro Peak.

6. There appears to be no appreciable difference in third-degree bias amplitude for the Landing Radar vector velocity magnitude obtained from the computer program for smooth and rough terrain as indicated in Figures 27 and 28.

7. Third-degree residuals for the Landing Radar vector velocity magnitude data versus polynomial fit appear to follow the same pattern as those for the cinetheodolite vector velocity magnitude data versus its polynomial fit for both smooth and rough terrain data as indicated in Figures 29 and 30.

8. Frequency tracker lag does not appear to be the cause of the observed slant range errors over rough terrain. Slant range errors predicted on the basis of a simplified tracker model are too small to account for the observed errors. In addition, the velocity dependence of the errors which would be expected in the case of dynamic lag is not observed.

9. Little Burro Peak terrain is not the worst case terrain since it tends to emphasize errors in slant range but not in velocity. Other rough terrain features could emphasize errors in velocity but not in slant range.

Table 1.

Landing Radar Specifications

FROM GAEC SPECIFICATION NO. LSP-470-2D,
MASTER END ITEM SPECIFICATION FOR LUNAR MODULE

Range Accuracy

| | |
|---|---|
| 2,000 ft. < R < 25,000 ft | 3 Sigma error = 1.4% + 15 ft |
| 10 ft. < R < 2,000 ft. | 3 Sigma error = 1.4% + 5 ft |

Velocity Accuracy to LGC (3 Sigma)

| Velocity Component | Altitude Range | | |
|---|---|---|---|
| | 25K ft. - 2K ft. | 2K ft. - 200 ft. | 200 ft. - 5 ft. |
| *$V_{xa}$ | 1.5% or 1.5 ft/sec | 1.5% or 1.5 ft/sec | 1.5% or 1.5 ft/sec |
| *$V_{ya}$ | 2.0% or 2.0 ft/sec | 3.5% or 3.5 ft/sec | 2.0% or 1.5 ft/sec |
| *$V_{za}$ | 2.0% or 2.0 ft/sec | 3.0% or 3.0 ft/sec | 2.0% or 1.5 ft/sec |

*Refer to % of Vector Velocity.

Note: Use % or ft/sec, whichever is greater.

Table 2. Comparison of LR Slant Range Errors with Specifications
LR-77E, Pass 1, RCT 78,476 to 78,536
T-33 Jet Profile Over Little Burro Peak

| Time Into Pass (sec) | Cine-theodolite Slant Range (feet) | Slant Range Error (LR-Cine) (feet) | Specified Error $3\sigma_s$ (feet) | Maximum Cine Error $3\sigma_c$ (feet) | Combined Spec $3\sigma_t$ $3\sigma_t = 3(\sigma_s^2 + \sigma_c^2)^{1/2}$ (feet) |
|---|---|---|---|---|---|
| 60 | 3565.6 | + 44.105 | 64.92 | 5.21 | 65.13 |
| 62 | 3530.5 | + 19.916 | 64.43 | 5.21 | 64.56 |
| 64 | 3433.2 | + 47.002 | 63.06 | 5.21 | 63.27 |
| 66 | 3337.0 | + 62.340 | 61.72 | 5.21 | 61.98 |
| 68 | 3232.4 | + 58.968 | 60.25 | 5.21 | 60.51 |
| 70 | 3126.2 | + 73.470 | 58.77 | 5.21 | 59.01 |
| 72 | 2952.9 | + 90.245 | 56.34 | 5.21 | 56.55 |
| 74 | 2711.0 | + 208.032 | 52.95 | 5.21 | 53.22 |
| 76 | 2405.3 | + 211.570 | 48.67 | 5.21 | 48.96 |
| 78 | 2139.1 | + 1.858 | 44.95 | 5.21 | 45.18 |
| 80 | 1855.1 | - 50.848 | 30.97 | 5.21 | 31.38 |
| 82 | 1646.8 | + 56.040 | 28.06 | 5.21 | 28.50 |
| 84 | 1978.9 | + 41.187 | 32.70 | 5.21 | 33.09 |
| 86 | 1595.9 | + 221.300 | 27.34 | 5.21 | 27.84 |
| 88 | 1145.1 | + 213.487 | 21.03 | 5.21 | 21.66 |
| 90 | 1330.6 | - 42.174 | 23.63 | 5.21 | 24.21 |
| 92 | 1719.8 | - 109.797 | 29.08 | 5.21 | 29.52 |
| 94 | 2103.5 | - 66.111 | 44.45 | 5.21 | 44.76 |
| 96 | 2029.1 | - 126.620 | 43.41 | 5.21 | 43.74 |
| 98 | 2459.4 | - 69.212 | 49.43 | 5.21 | 49.74 |
| 100 | 2841.6 | - 96.394 | 54.78 | 5.21 | 55.05 |
| 102 | 3035.5 | - 20.453 | 57.50 | 5.51 | 57.75 |
| 104 | 3192.0 | + 25.881 | 59.69 | 5.21 | 60.00 |
| 106 | 3353.0 | - 2.263 | 61.94 | 5.21 | 62.10 |
| 108 | 3455.0 | + 3.692 | 63.37 | 5.21 | 63.60 |
| 110 | 3491.0 | + 43.204 | 63.87 | 5.21 | 65.10 |
| 112 | 3553.1 | + 18.863 | 64.74 | 5.21 | 64.86 |
| 114 | 3607.3 | + 56.399 | 65.50 | 5.21 | 65.67 |
| 116 | 3664.2 | + 15.618 | 66.30 | 5.21 | 66.57 |
| 118 | 3708.0 | + 36.619 | 66.91 | 5.21 | 67.17 |
| 120 | 3744.5 | + 43.312 | 67.42 | 5.21 | 67.56 |

Table 3. Comparison of LR Slant Range Errors with Specifications

LR-58E, Pass 2, RCT 72,521 to 72,681 SH-3A Helicopter
Profile Over Little Burro Peak

| Time Into Pass (sec) | Cine-theodolite Slant Range (feet) | Slant Range Error (LR-Cine) (feet) | Specified Error $3\sigma_s$ (feet) | Maximum Cine Error $3\sigma_c$ (feet) | Combined Spec $3\sigma_t$ $3\sigma_t = 3(\sigma_s^2 + \sigma_c^2)^{1/2}$ (feet) |
|---|---|---|---|---|---|
| 120 | 2455.2 | 120.635 | 49.37 | 5.88 | 49.72 |
| 122 | 2363.9 | 97.546 | 48.09 | 5.88 | 48.45 |
| 124 | 2297.5 | 26.930 | 47.16 | 5.88 | 47.53 |
| 126 | 2260.0 | 105.417 | 46.64 | 5.88 | 47.01 |
| 128 | 2229.3 | 82.084 | 46.21 | 5.88 | 46.58 |
| 130 | 2189.4 | 103.669 | 45.65 | 5.88 | 46.03 |
| 132 | 2196.9 | 127.447 | 45.76 | 5.88 | 46.13 |
| 134 | 2122.2 | 119.122 | 44.71 | 5.88 | 45.10 |
| 136 | 2065.1 | 101.698 | 43.91 | 5.88 | 44.30 |
| 138 | 2047.7 | 52.272 | 43.67 | 5.88 | 44.06 |
| 140 | 2127.0 | - 97.193 | 44.78 | 5.88 | 45.16 |
| 142 | 2185.6 | - 95.403 | 45.60 | 5.88 | 45.98 |
| 144 | 2347.3 | - 181.563 | 47.86 | 5.88 | 48.22 |
| 146 | 2215.5 | 48.477 | 46.02 | 5.88 | 46.39 |
| 148 | 2159.9 | 169.832 | 45.24 | 5.88 | 45.62 |
| 150 | 2186.8 | 178.542 | 45.62 | 5.88 | 45.99 |
| 152 | 2203.4 | 171.667 | 45.85 | 5.88 | 46.22 |
| 154 | 2209.9 | 92.857 | 45.94 | 5.88 | 46.31 |
| 156 | 2192.7 | 105.738 | 45.70 | 5.88 | 46.07 |
| 158 | 2177.1 | 117.035 | 45.48 | 5.88 | 45.86 |
| 160 | 2217.5 | 105.775 | 46.05 | 5.88 | 46.42 |
| 162 | 2167.9 | 114.390 | 44.00 | 5.88 | 44.39 |
| 164 | 2071.4 | 90.081 | 43.19 | 5.88 | 43.59 |
| 166 | 2013.6 | 65.872 | 31.85 | 5.88 | 32.39 |
| 168 | 1917.8 | 24.534 | 31.19 | 5.88 | 31.74 |
| 170 | 1890.6 | 53.915 | 31.80 | 5.88 | 32.31 |
| 172 | 1835.3 | 105.969 | 30.69 | 5.88 | 31.25 |
| 174 | 1799.3 | 153.899 | 30.19 | 5.88 | 30.76 |
| 176 | 1800.6 | 179.568 | 30.21 | 5.88 | 30.78 |
| 178 | 1793.2 | 167.505 | 30.10 | 5.88 | 30.67 |
| 180 | 1748.1 | 179.221 | 29.47 | 5.88 | 30.05 |
| 182 | 1691.2 | 182.123 | 28.68 | 5.88 | 29.27 |
| 184 | 1636.0 | 140.219 | 27.90 | 5.88 | 28.52 |
| 186 | 1570.7 | 92.230 | 26.99 | 5.88 | 27.62 |
| 188 | 1514.7 | - 39.587 | 26.21 | 5.88 | 26.86 |
| 190 | 1496.1 | - 53.385 | 25.95 | 5.88 | 26.60 |
| 192 | 1500.5 | + 14.513 | 26.01 | 5.88 | 26.66 |
| 194 | 1557.9 | 37.040 | 26.81 | 5.88 | 27.45 |
| 196 | 1610.6 | 50.122 | 27.55 | 5.88 | 28.17 |
| 198 | 1668.8 | 62.091 | 28.36 | 5.88 | 28.97 |

Table 3. (Continued)

| Time Into Pass (sec) | Cine-theodolite Slant Range (feet) | Slant Range Error (LR-Cine) (feet) | Specified Error $3\sigma_s$ (feet) | Maximum Cine Error $3\sigma_c$ (feet) | Combined Spec $3\sigma_t$ $3\sigma_t = 3(\sigma_s^2 + \sigma_c^2)^{1/2}$ (feet) |
|---|---|---|---|---|---|
| 120 | 2455.2 | 120.635 | 49.37 | 5.88 | 49.72 |
| 122 | 2363.9 | 97.546 | 48.09 | 5.88 | 48.45 |
| 124 | 2297.5 | 26.930 | 47.16 | 5.88 | 47.53 |
| 126 | 2260.0 | 105.417 | 46.64 | 5.88 | 47.01 |
| 128 | 2229.3 | 82.084 | 46.21 | 5.88 | 46.58 |
| 130 | 2189.4 | 103.669 | 45.65 | 5.88 | 46.03 |
| 132 | 2196.9 | 127.447 | 45.76 | 5.88 | 46.13 |
| 134 | 2122.2 | 119.122 | 44.71 | 5.88 | 45.10 |
| 136 | 2065.1 | 101.698 | 43.91 | 5.88 | 44.30 |
| 138 | 2047.7 | 52.272 | 43.67 | 5.88 | 44.06 |
| 140 | 2127.0 | - 97.193 | 44.78 | 5.88 | 45.16 |
| 142 | 2185.6 | - 95.403 | 45.60 | 5.88 | 45.98 |
| 144 | 2347.3 | - 181.563 | 47.86 | 5.88 | 48.22 |
| 146 | 2215.5 | 48.477 | 46.02 | 5.88 | 46.39 |
| 148 | 2159.9 | 169.832 | 45.24 | 5.88 | 45.62 |
| 150 | 2186.8 | 178.542 | 45.62 | 5.88 | 45.99 |
| 152 | 2203.4 | 171.667 | 45.85 | 5.88 | 46.22 |
| 154 | 2209.9 | 92.857 | 45.94 | 5.88 | 46.31 |
| 156 | 2192.7 | 105.738 | 45.70 | 5.88 | 46.07 |
| 158 | 2177.1 | 117.035 | 45.48 | 5.88 | 45.86 |
| 160 | 2217.5 | 105.775 | 46.05 | 5.88 | 46.42 |
| 162 | 2167.9 | 114.390 | 44.00 | 5.88 | 44.39 |
| 164 | 2071.4 | 90.081 | 43.19 | 5.88 | 43.59 |
| 166 | 2013.6 | 65.872 | 31.85 | 5.88 | 32.39 |
| 168 | 1917.8 | 24.534 | 31.19 | 5.88 | 31.74 |
| 170 | 1890.6 | 53.915 | 31.80 | 5.88 | 32.31 |
| 172 | 1835.3 | 105.969 | 30.69 | 5.88 | 31.25 |
| 174 | 1799.3 | 153.899 | 30.19 | 5.88 | 30.76 |
| 176 | 1800.6 | 179.568 | 30.21 | 5.88 | 30.78 |
| 178 | 1793.2 | 167.505 | 30.10 | 5.88 | 30.67 |
| 180 | 1748.1 | 179.221 | 29.47 | 5.88 | 30.05 |
| 182 | 1691.2 | 182.123 | 28.68 | 5.88 | 29.27 |
| 184 | 1636.0 | 140.219 | 27.90 | 5.88 | 28.52 |
| 186 | 1570.7 | 92.230 | 26.99 | 5.88 | 27.62 |
| 188 | 1514.7 | - 39.587 | 26.21 | 5.88 | 26.86 |
| 190 | 1496.1 | - 53.385 | 25.95 | 5.88 | 26.60 |
| 192 | 1500.5 | + 14.513 | 26.01 | 5.88 | 26.66 |
| 194 | 1557.9 | 37.040 | 26.81 | 5.88 | 27.45 |
| 196 | 1610.6 | 50.122 | 27.55 | 5.88 | 28.17 |
| 198 | 1668.8 | 62.091 | 28.36 | 5.88 | 28.97 |

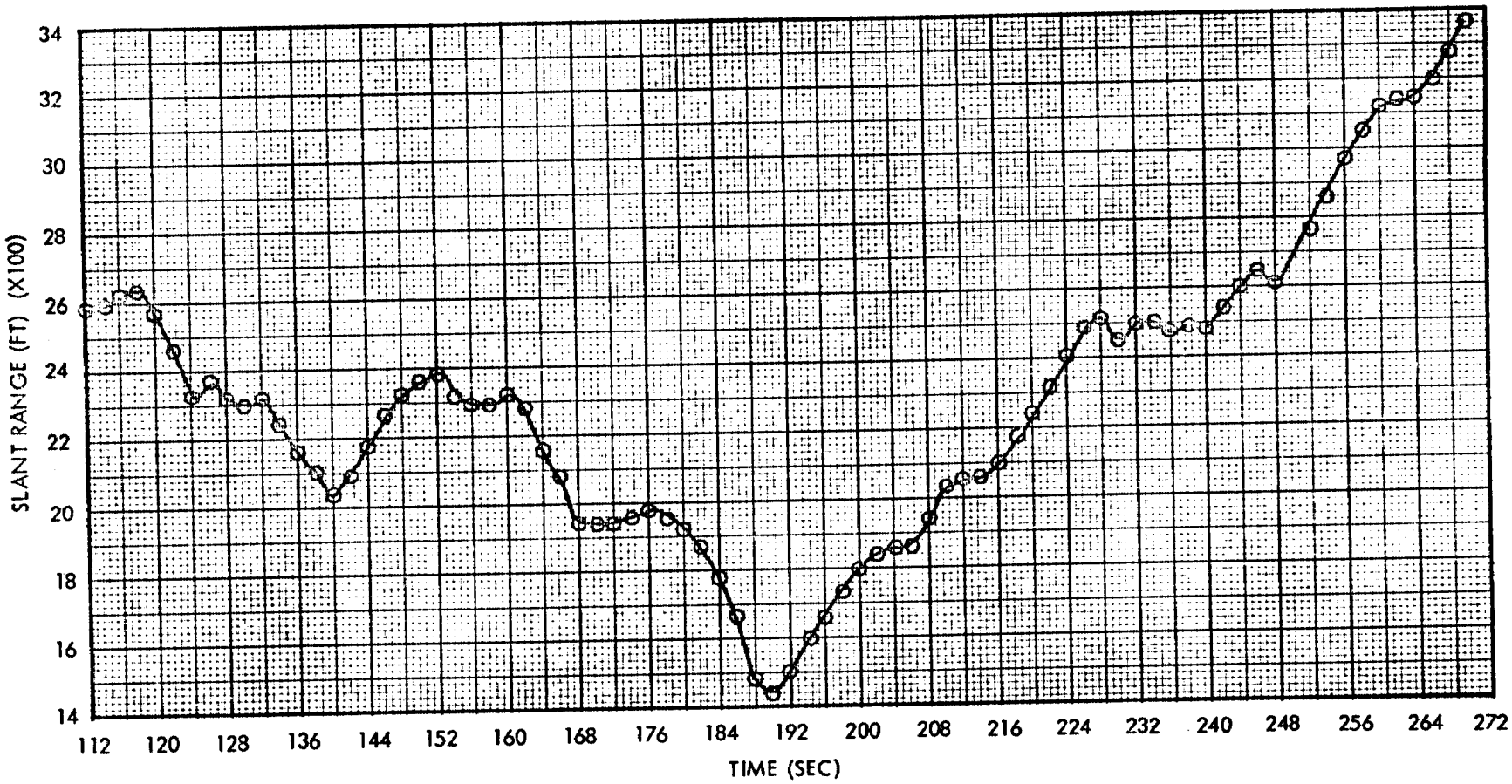


Figure 1. LR-58E, Pass 2, Landing Radar Slant Range

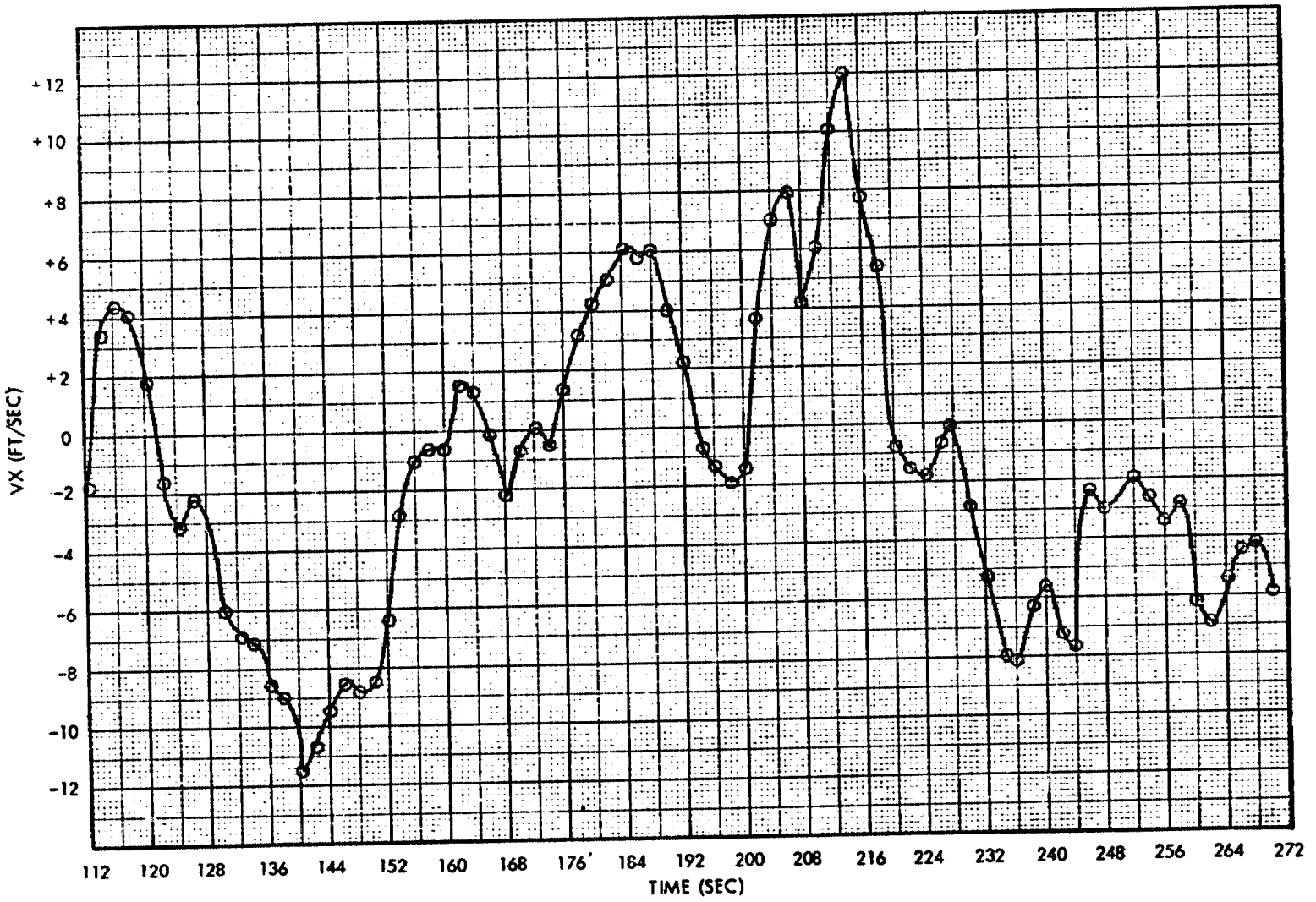


Figure 2. LR-58E, Pass 2, Landing Radar $V_x$ Component Velocity

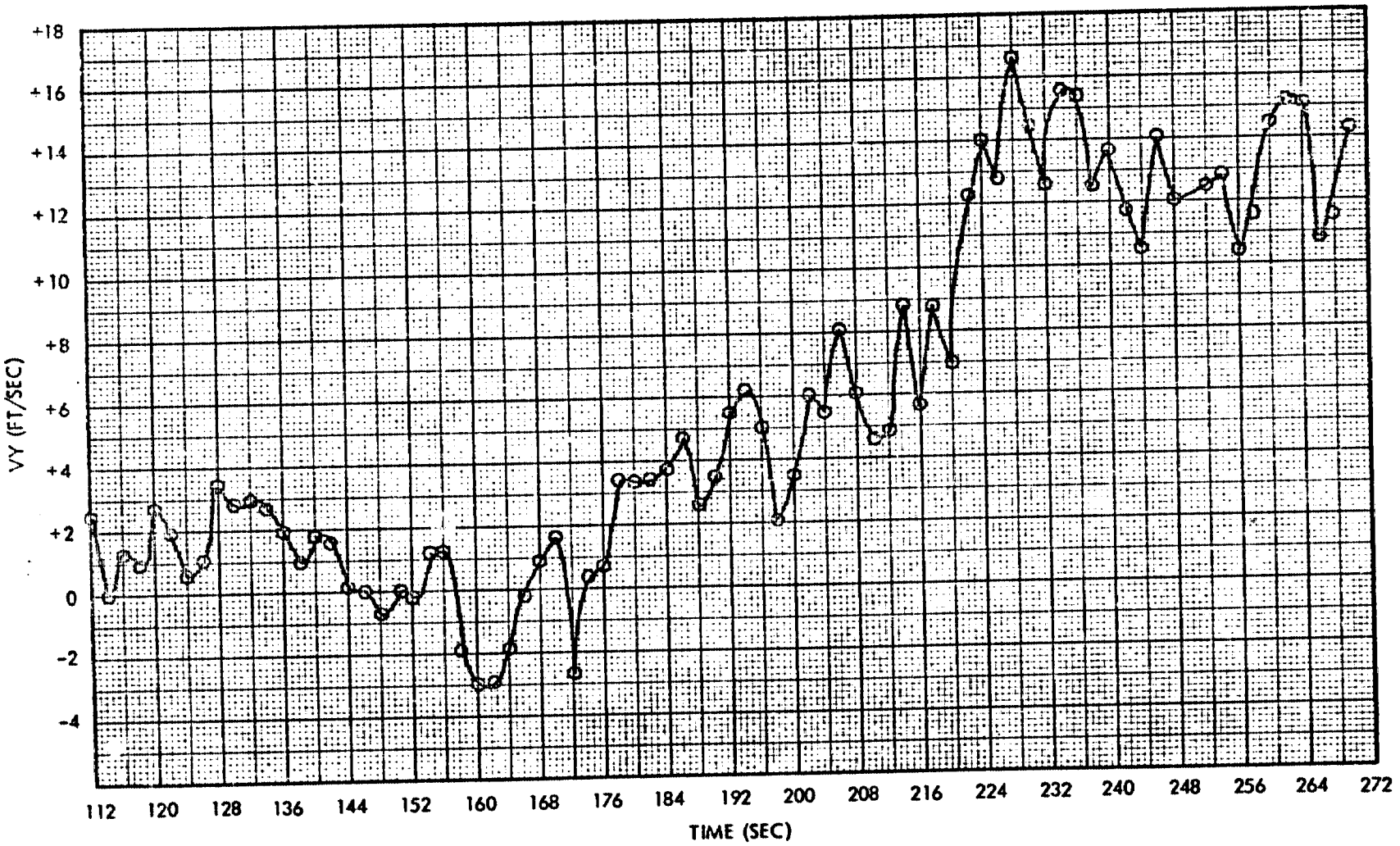


Figure 3. LR-58E, Pass 2, Landing Radar $V_y$ Component Velocity

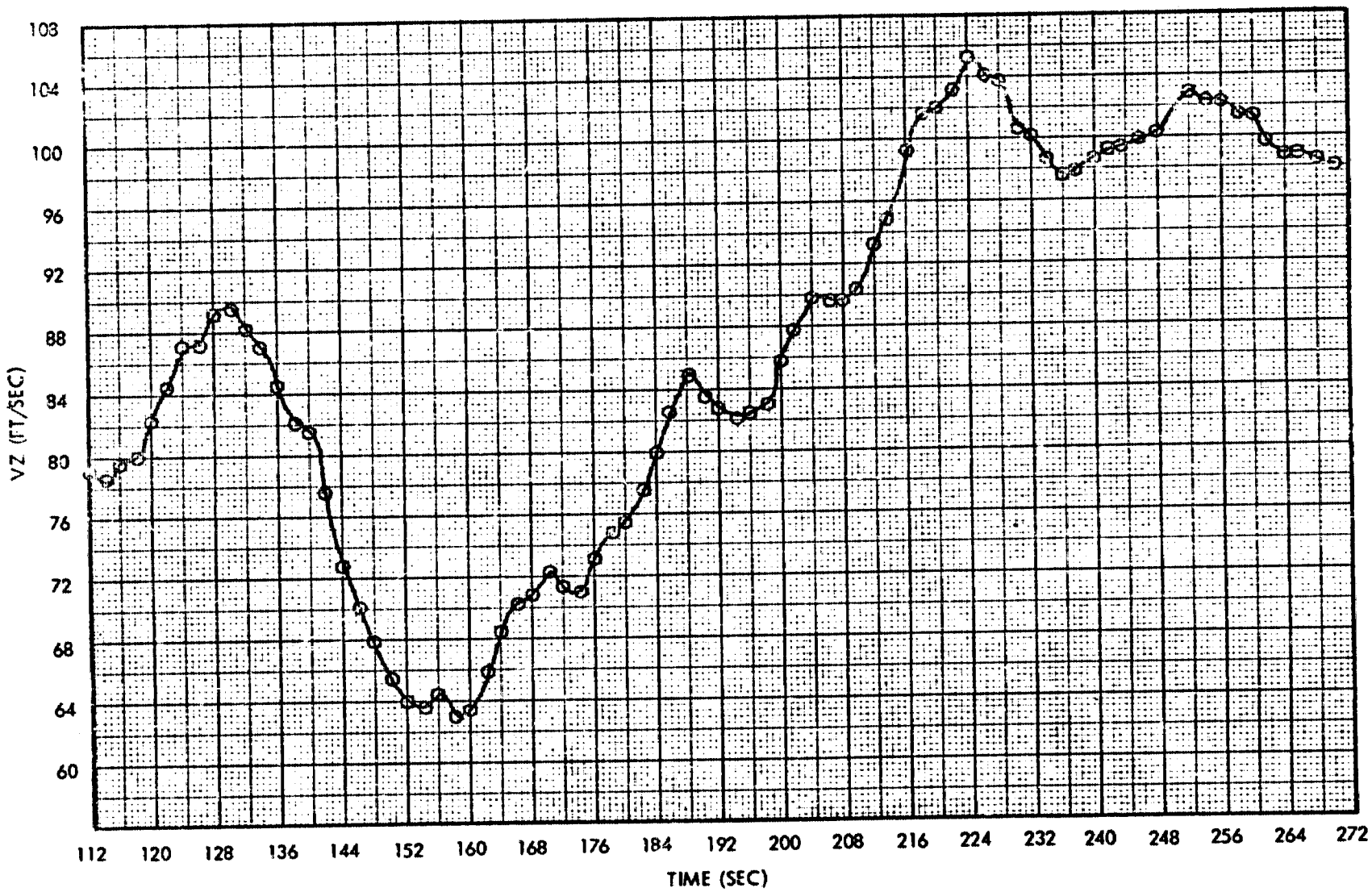


Figure 4. LR-58E, Pass 2, Landing Radar $V_z$ Component Velocity

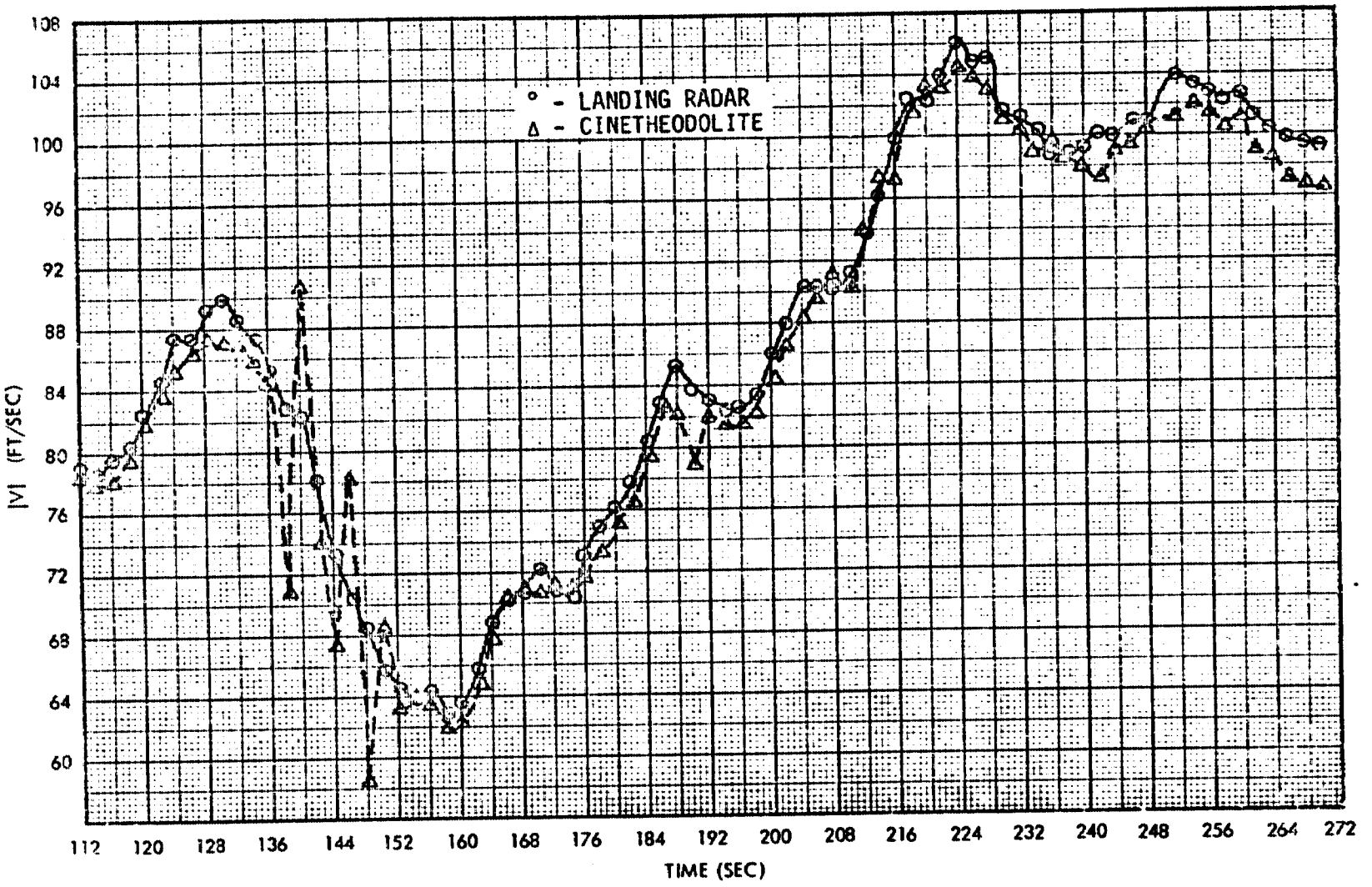


Figure 5. LR-58E, Pass 2, Landing Radar vs Cinetheodolite Vector Velocity

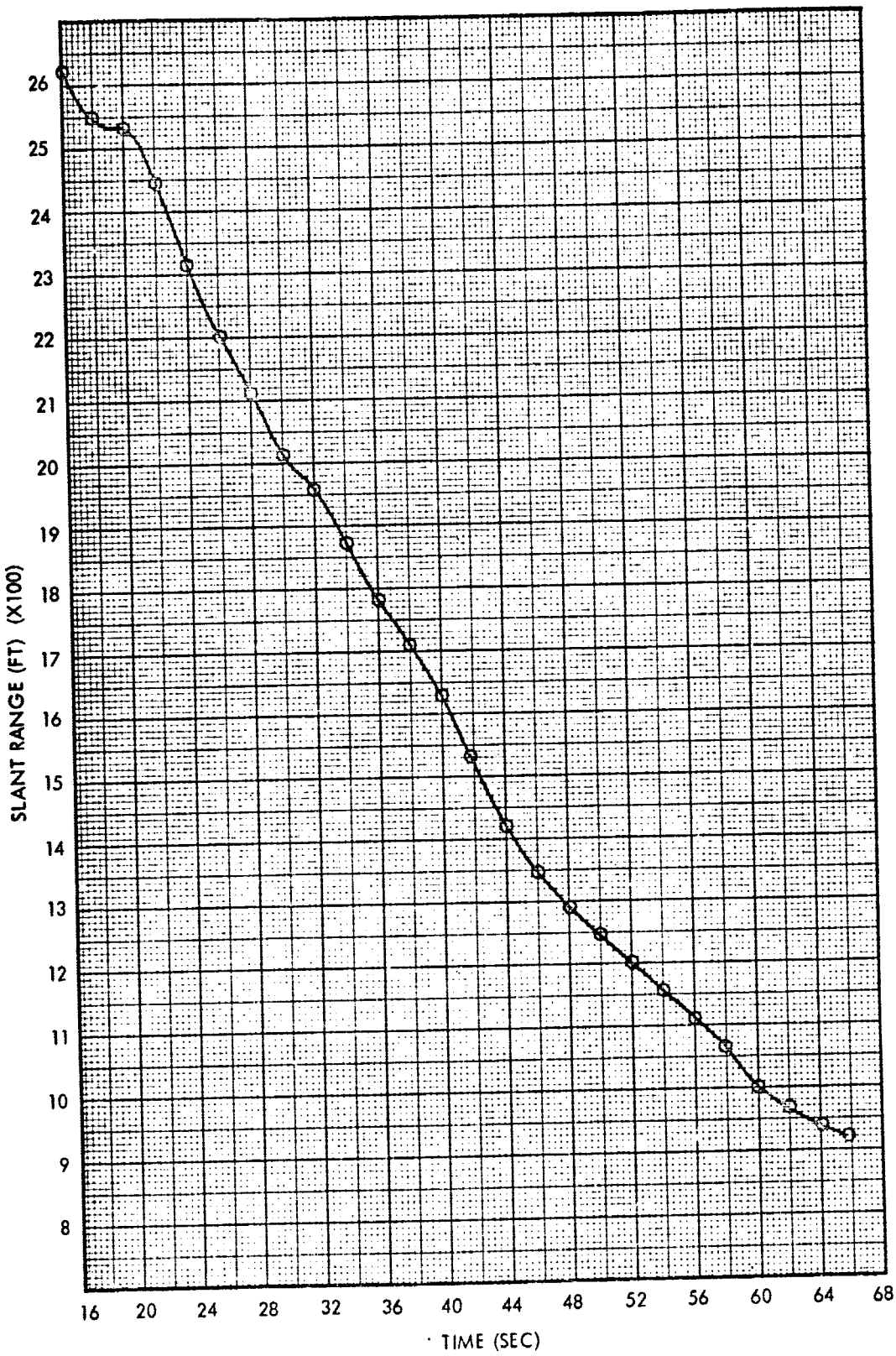


Figure 6. LR-60J, Pass 7, Landing Radar Slant Range

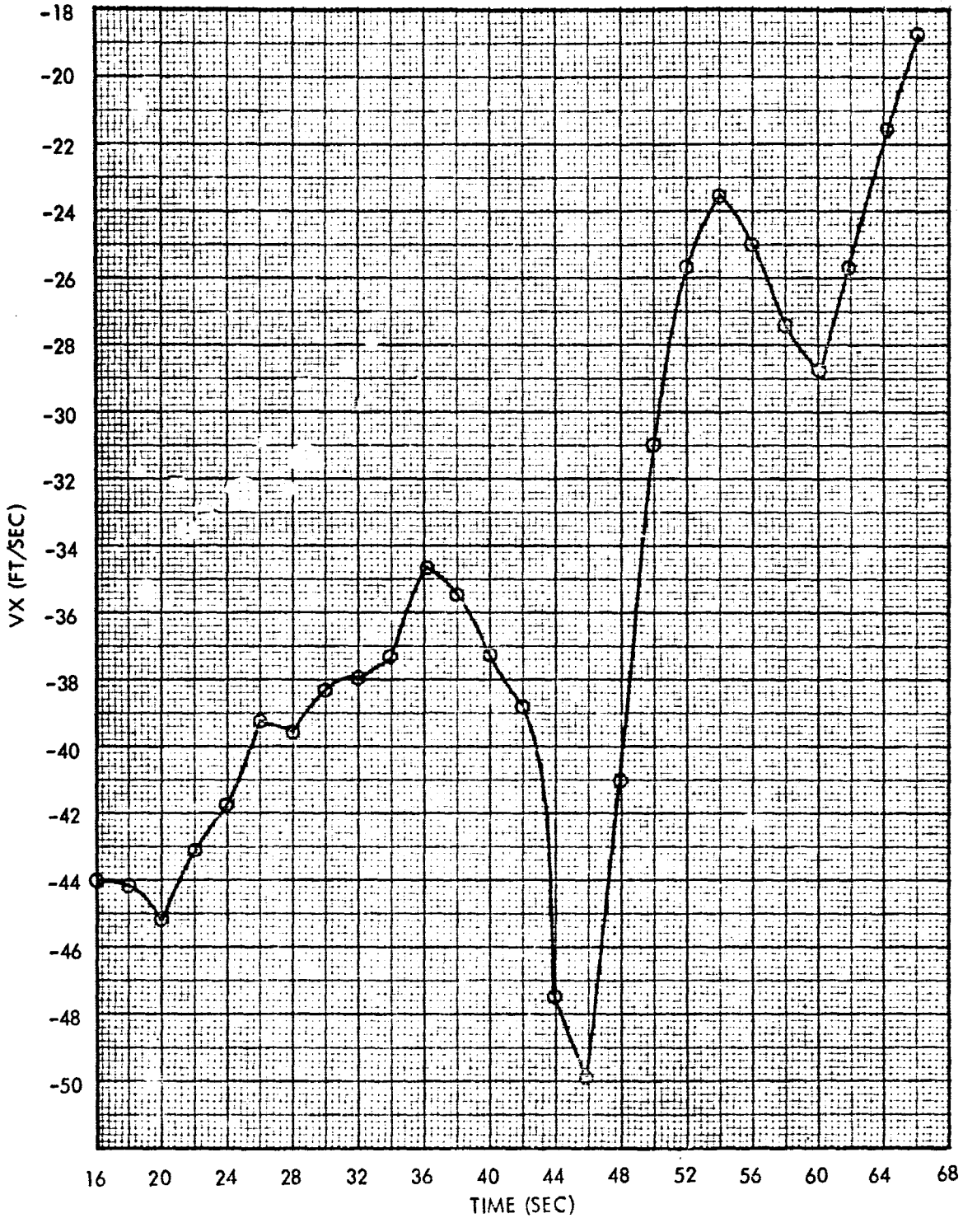


Figure 7. LR-60J, Pass 7, Landing Radar $V_x$ Component Velocity

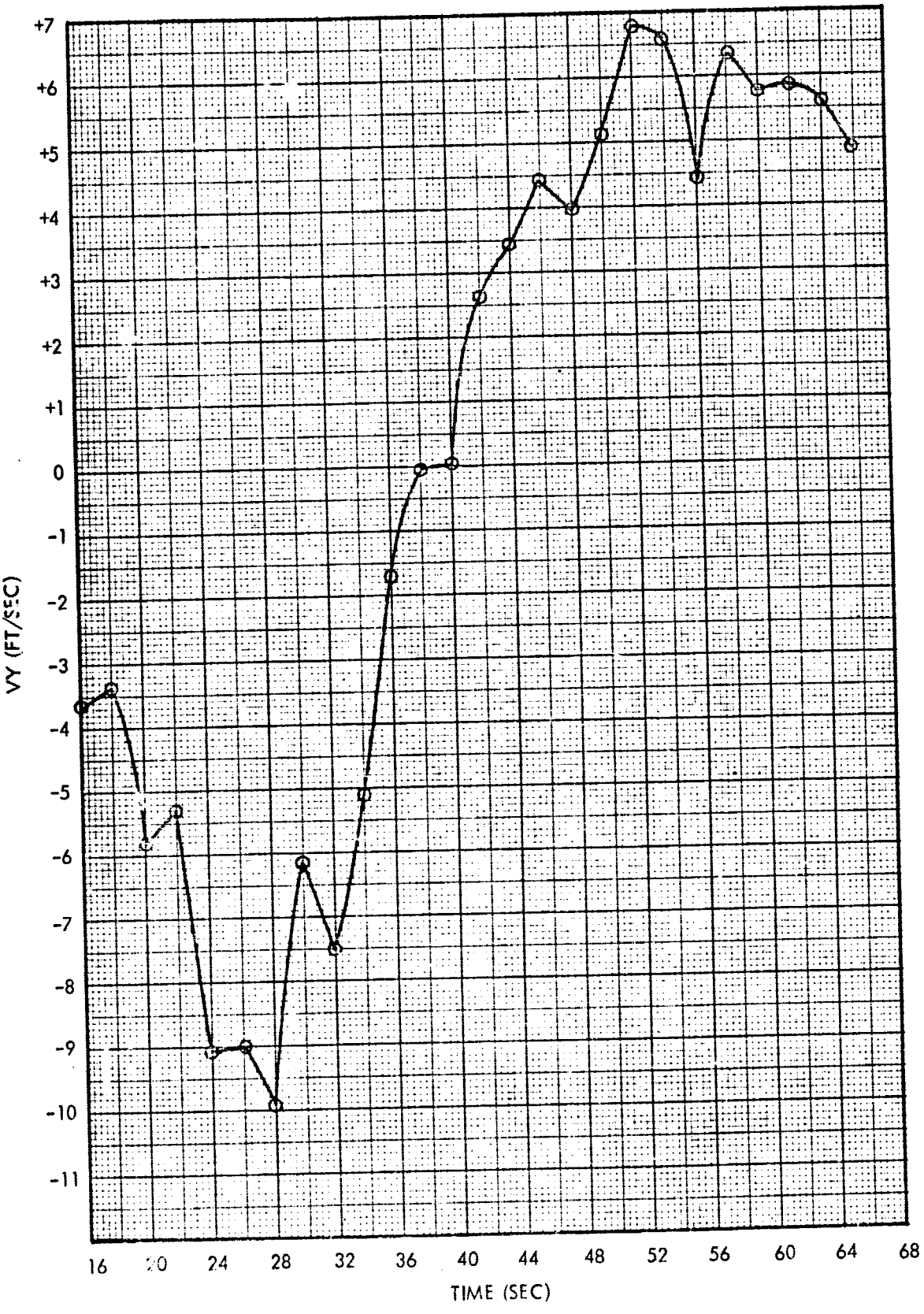


Figure 8. LR-60J, Pass 7, Landing Radar $V_y$ Component Velocity

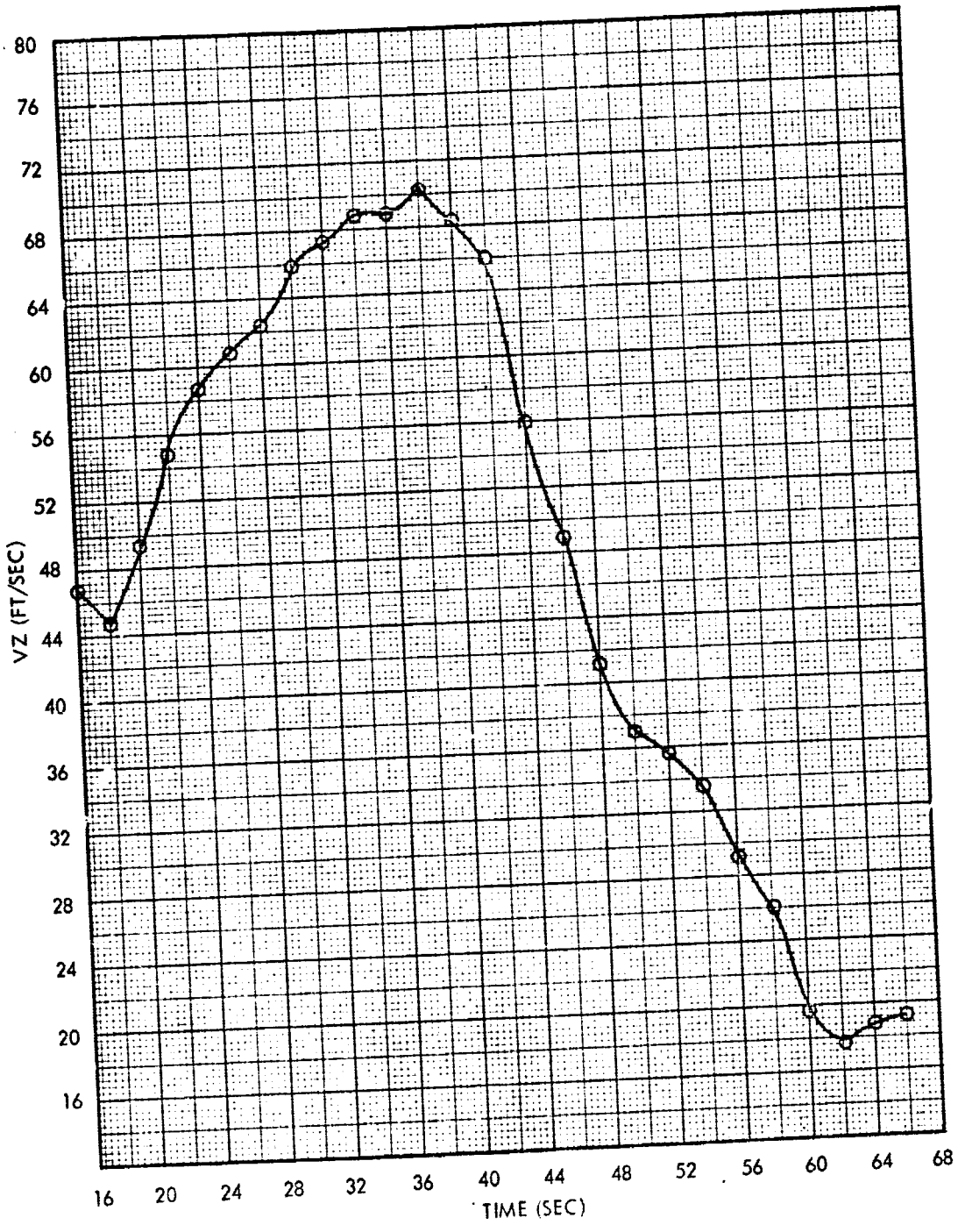


Figure 9. LR-60J, Pass 7, Landing Radar $V_Z$ Component Velocity

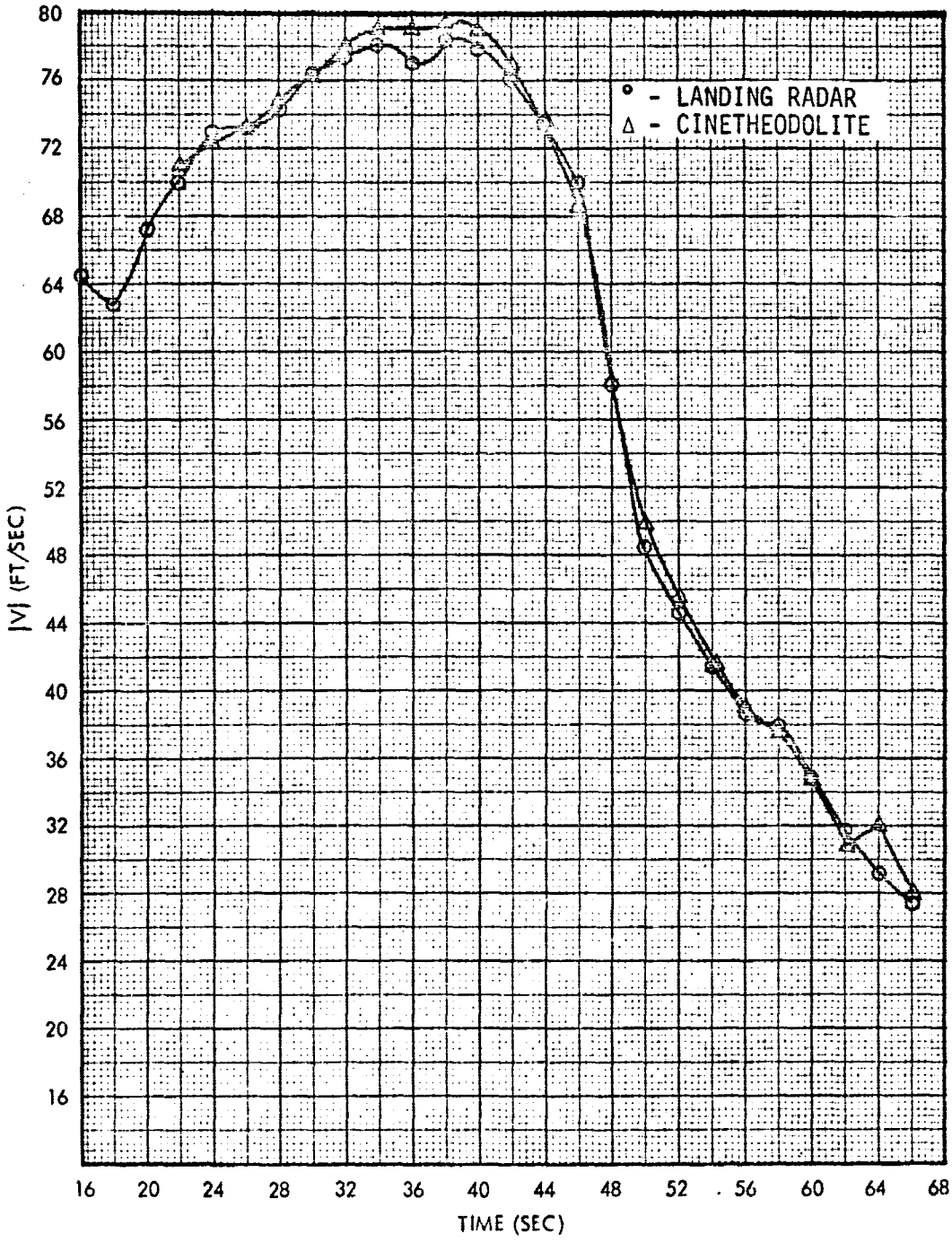


Figure 10. LR-60J, Pass 7, Landing Radar vs Cinetheodolite Vector Velocity

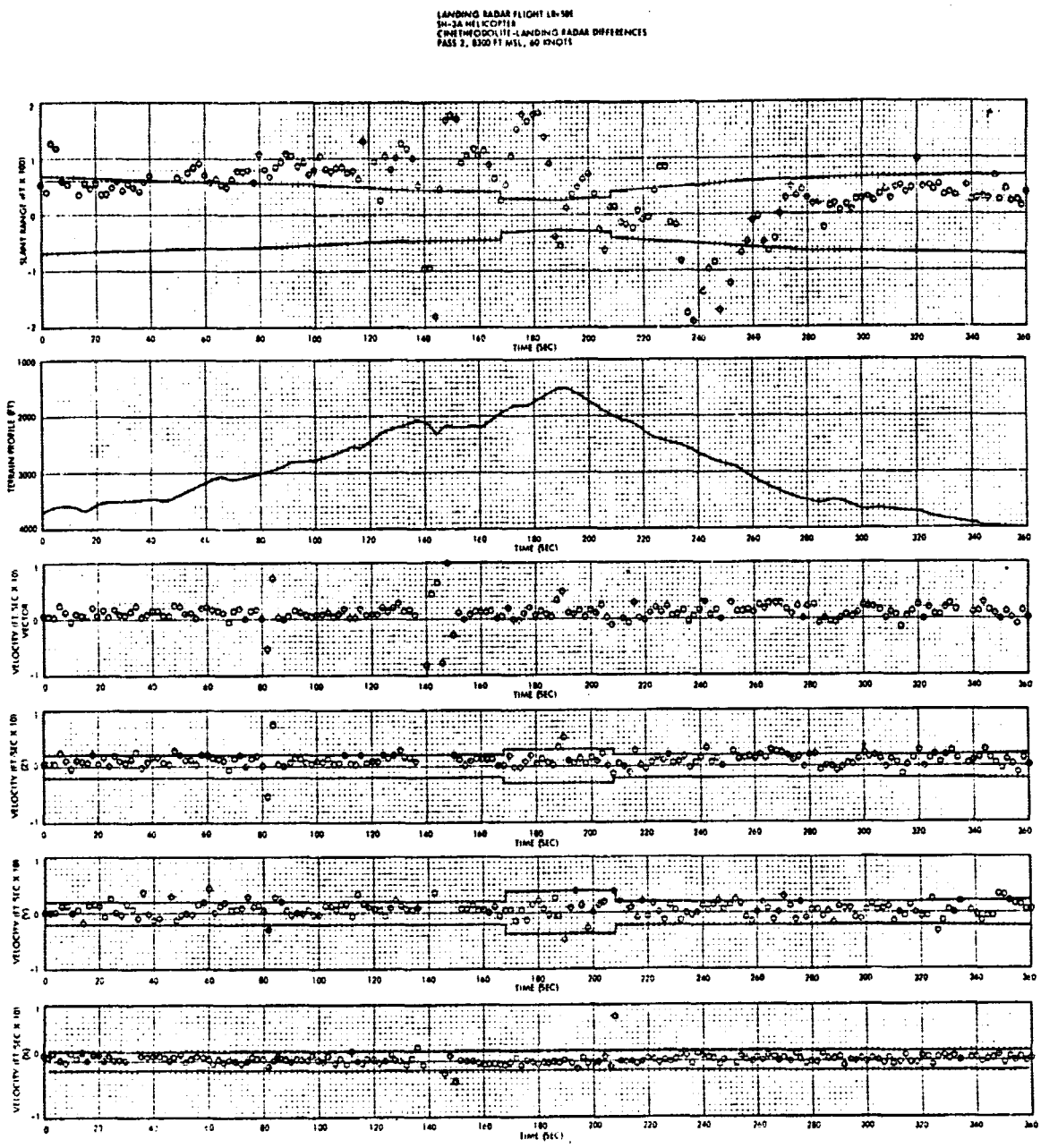


Figure 11. LR-58E, Pass 2, Cinetheodolite-Landing Radar Differences

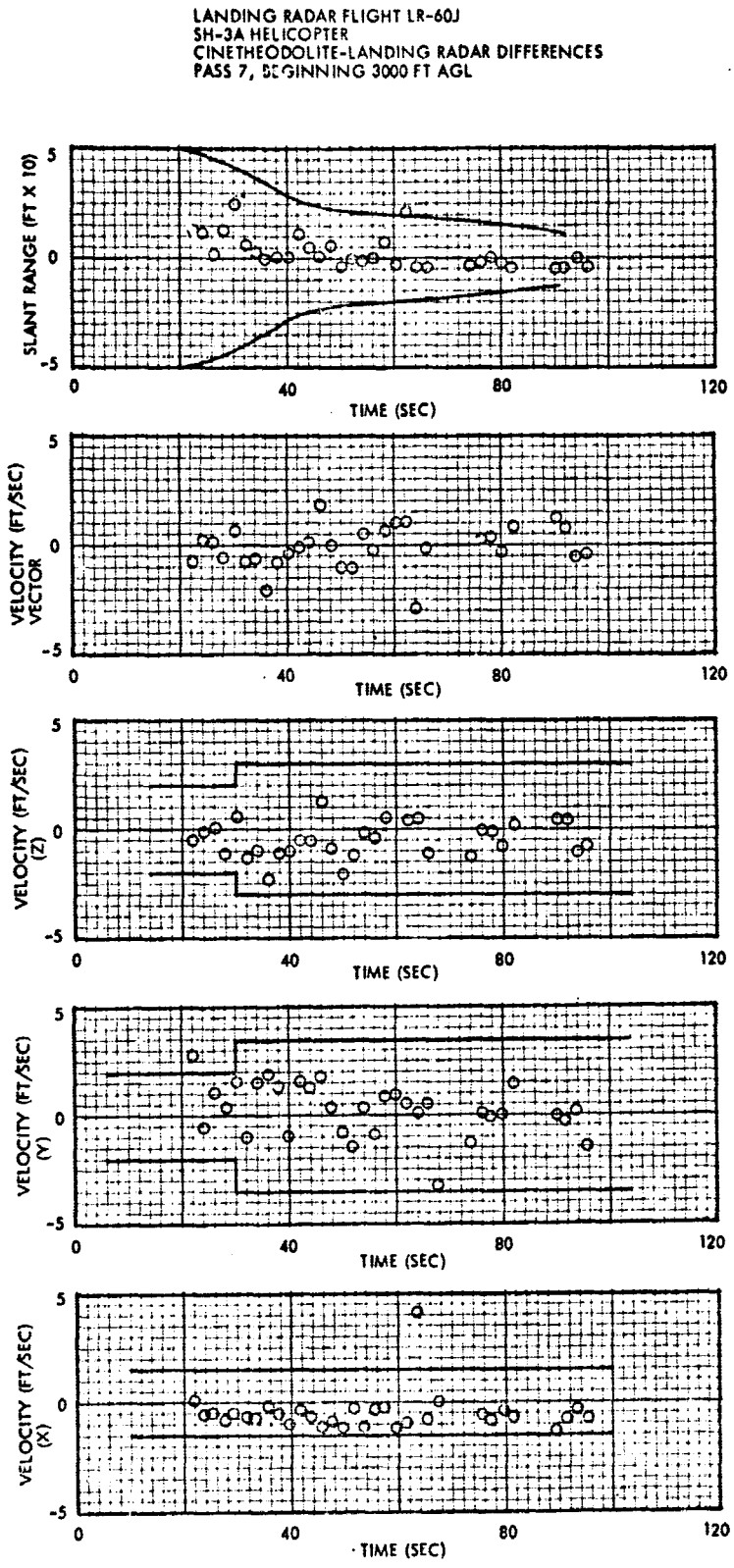


Figure 12. LR-60J, Pass 7, Cinetheodolite-Landing Radar Differences

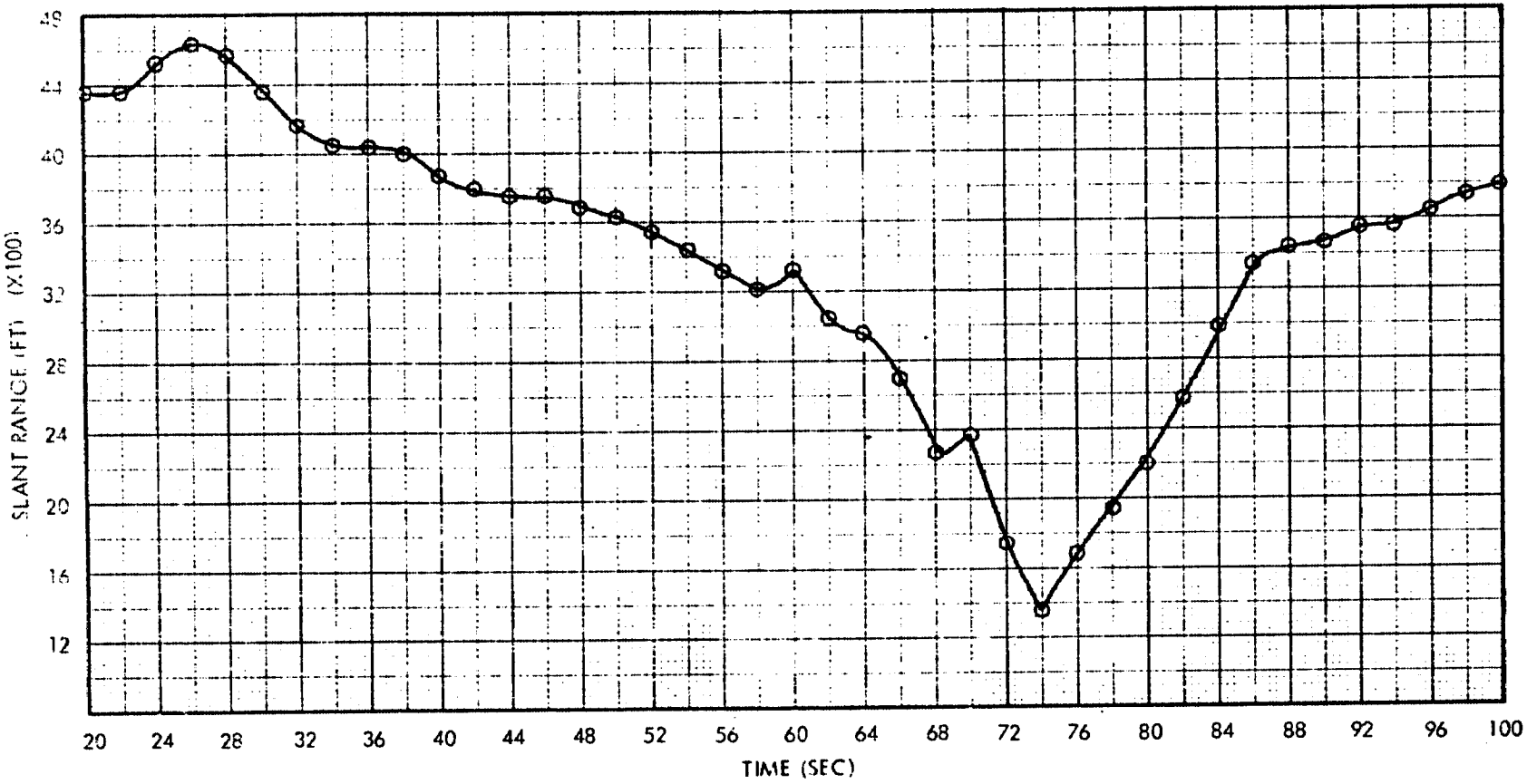


Figure 13. LR-77E, Pass 3, Landing Radar Slant Range

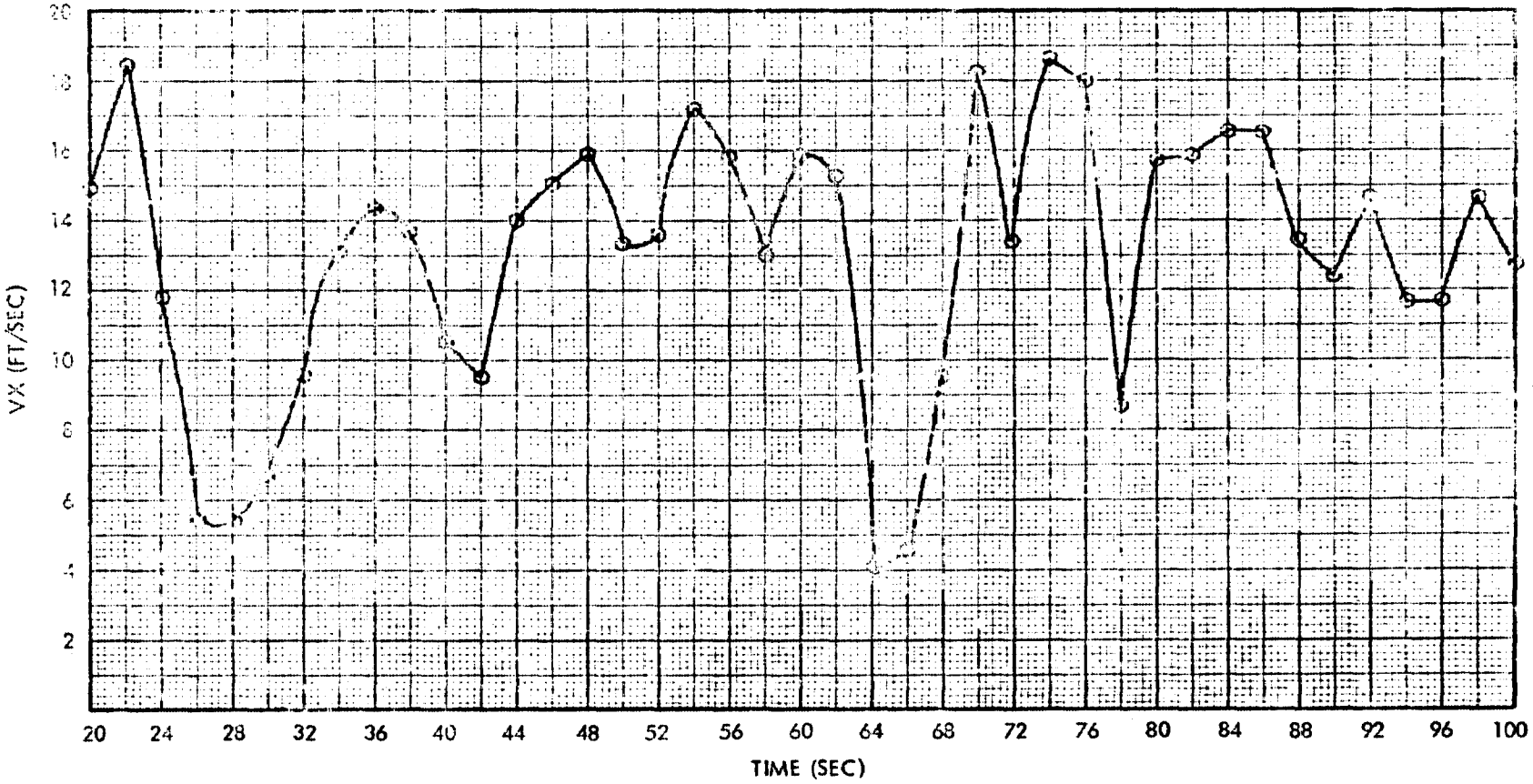


Figure 14. LR-77E, Pass 3, Landing Radar $V_X$ Component Velocity

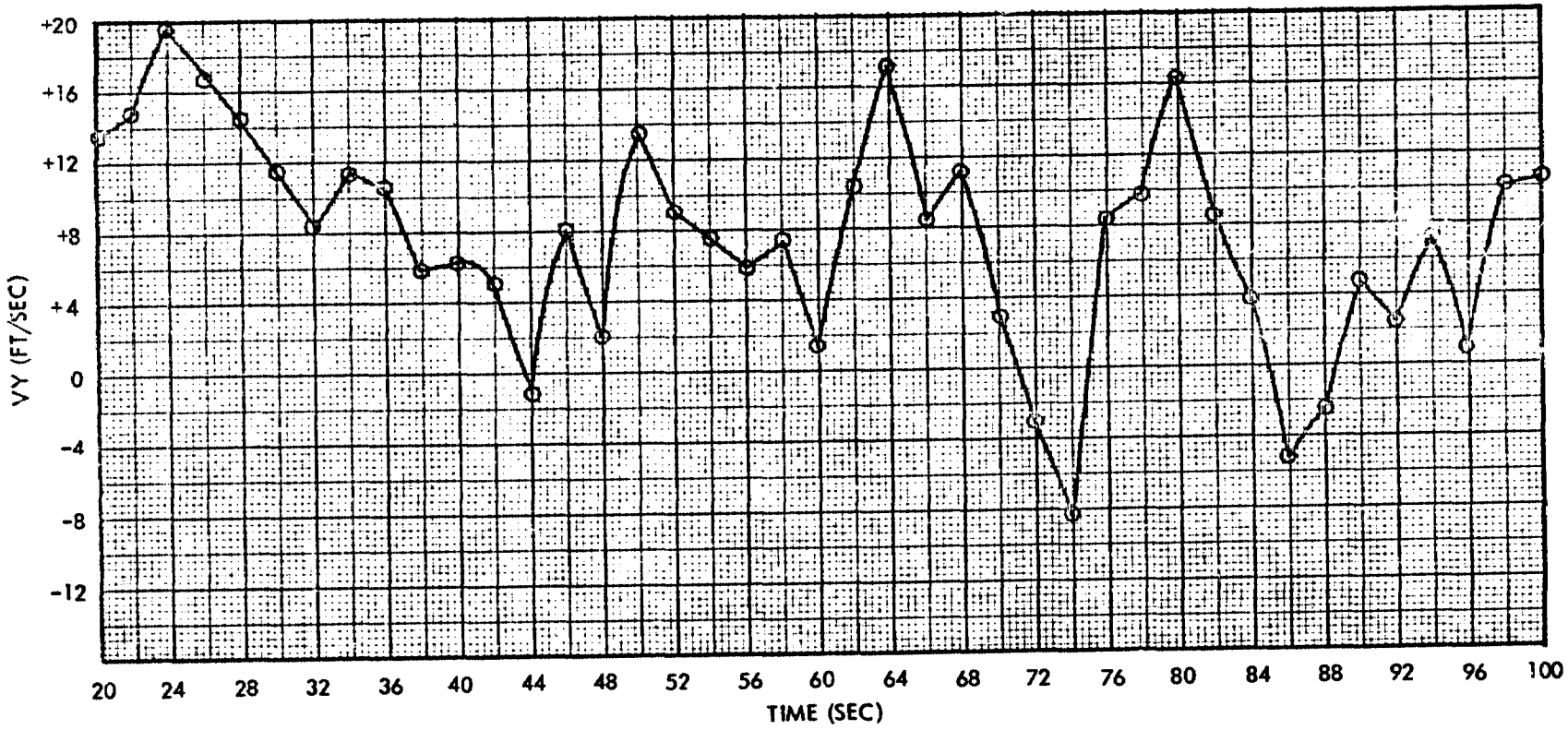


Figure 15. LR-77E, Pass 3, Landing Radar $V_y$ Component Velocity

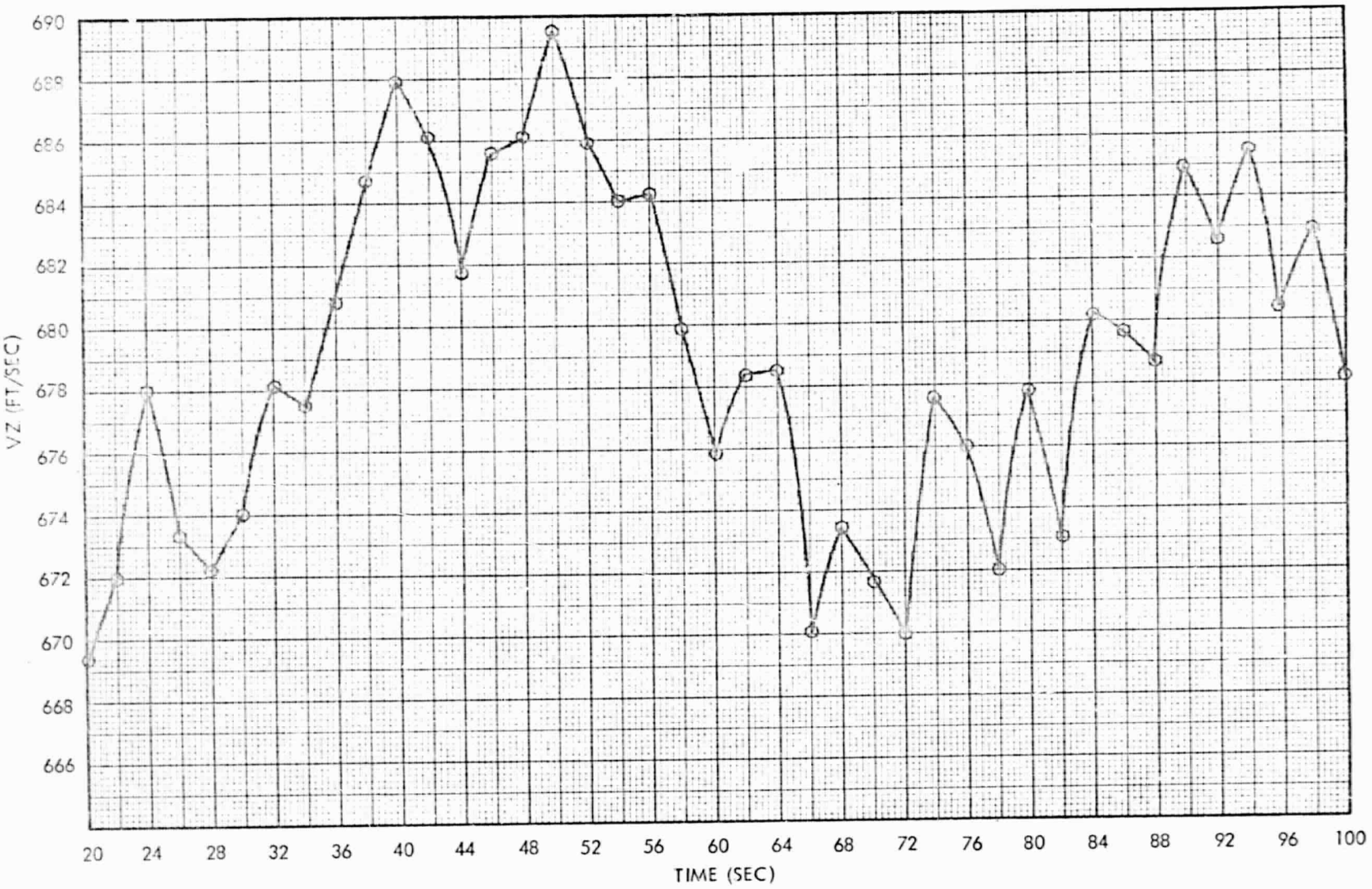


Figure 16. LR-77E, Pass 3, Landing Radar $V_z$ Component Velocity

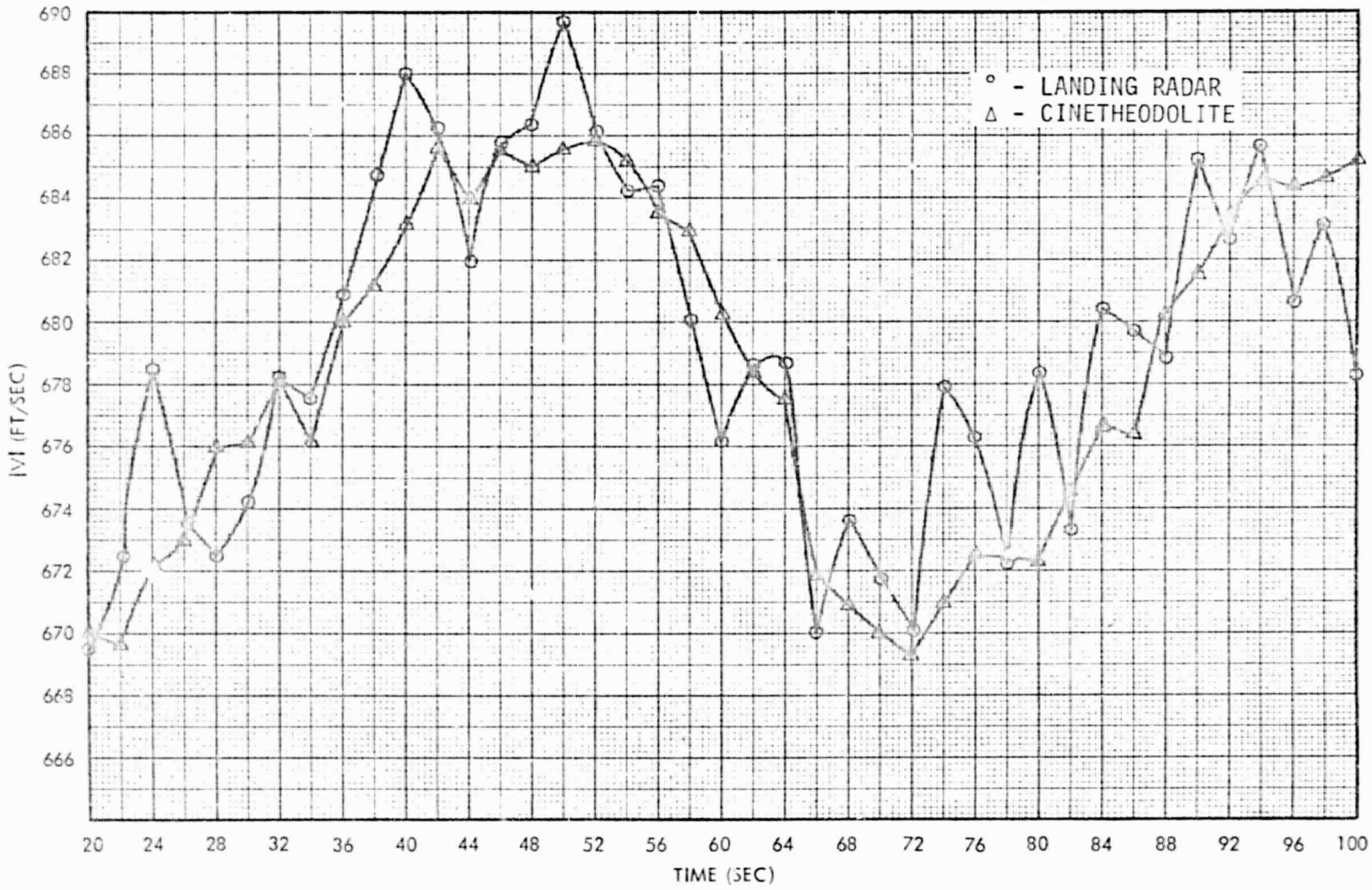


Figure 17. LR-77E, Pass 3, Landing Radar vs Cinetheodolite Vector Velocity

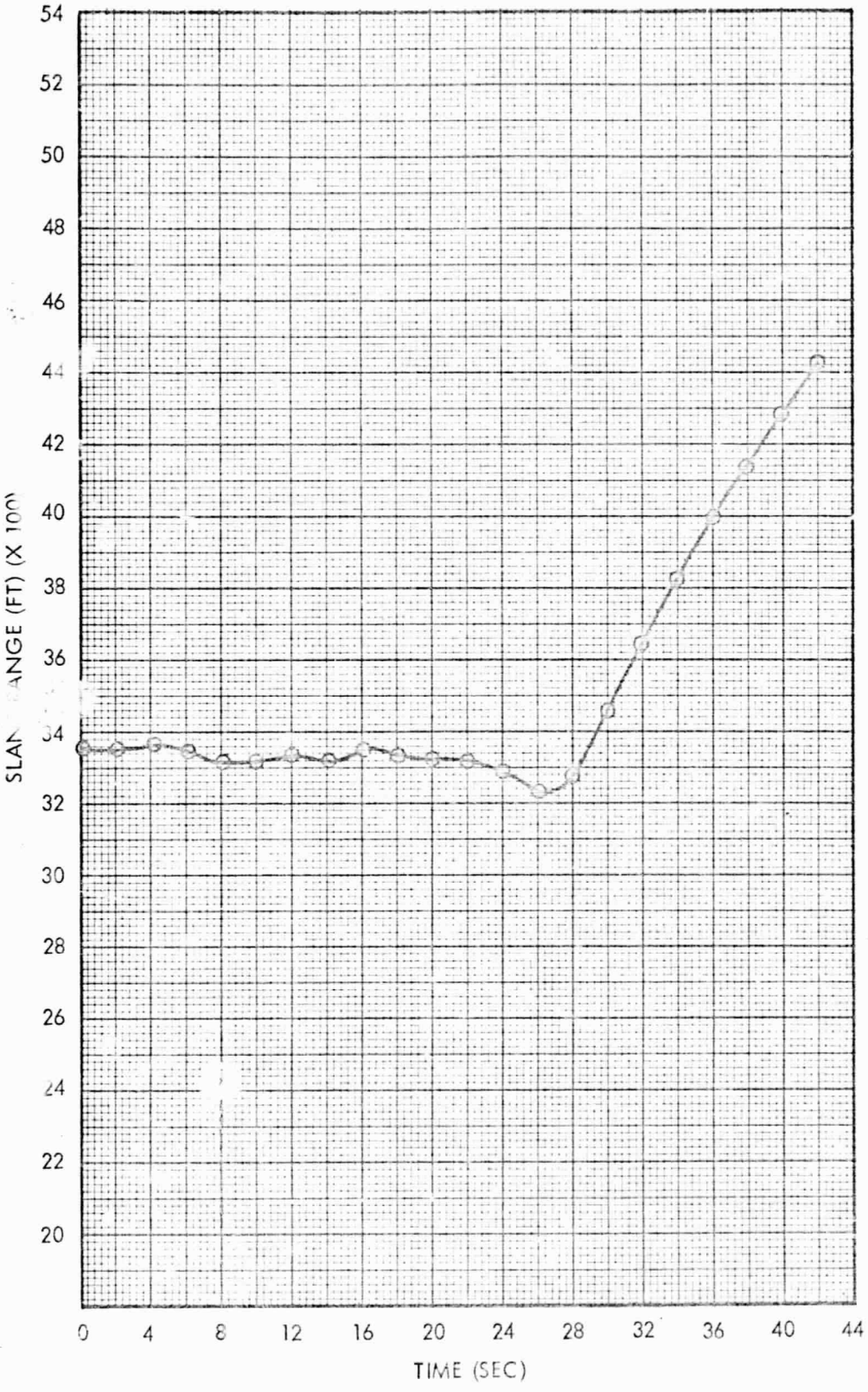


Figure 18. LR-73F, Pass 1, Landing Radar Slant Range

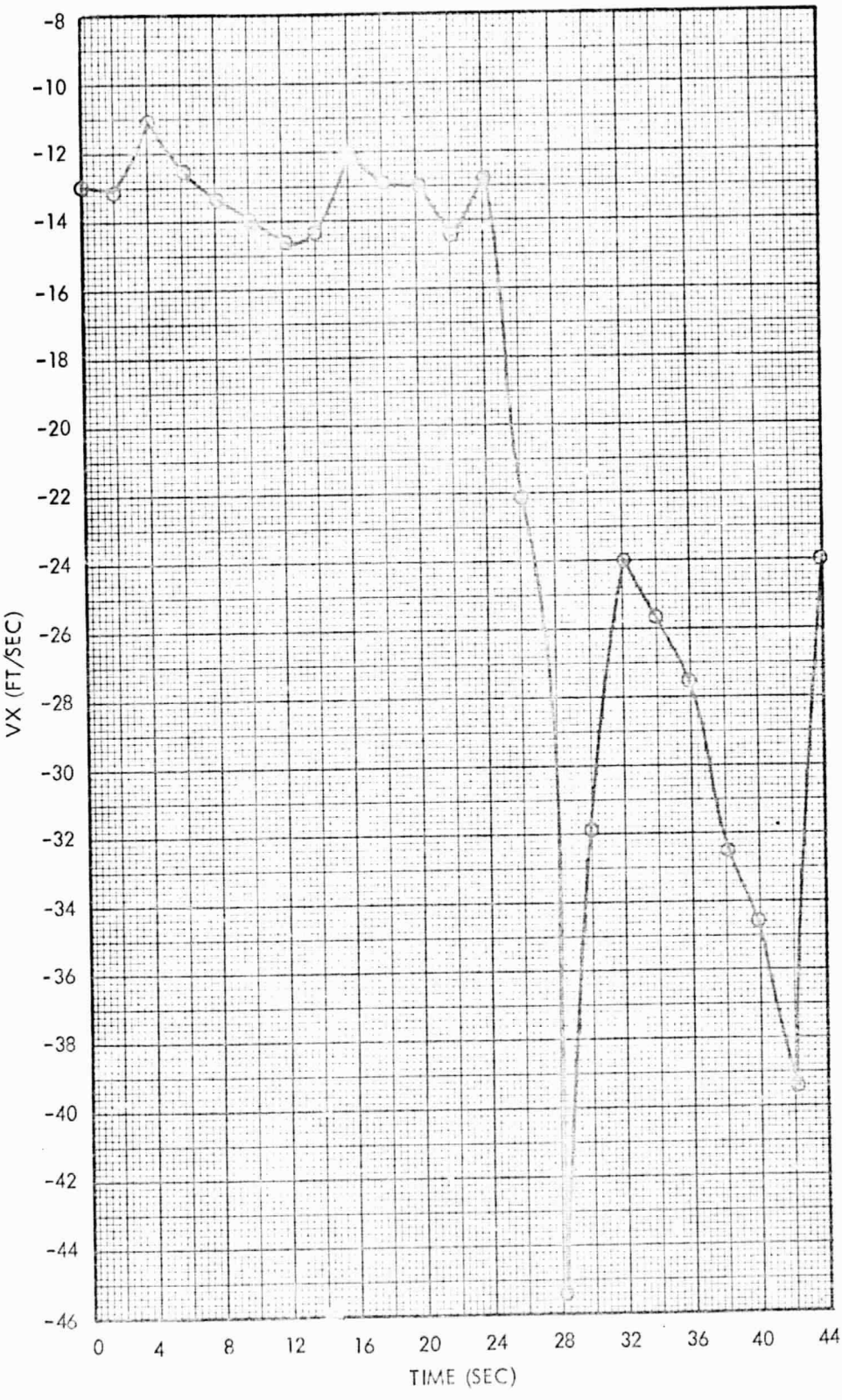


Figure 19. LR-73F, Pass 1, Landing Radar $V_X$ Component Velocity

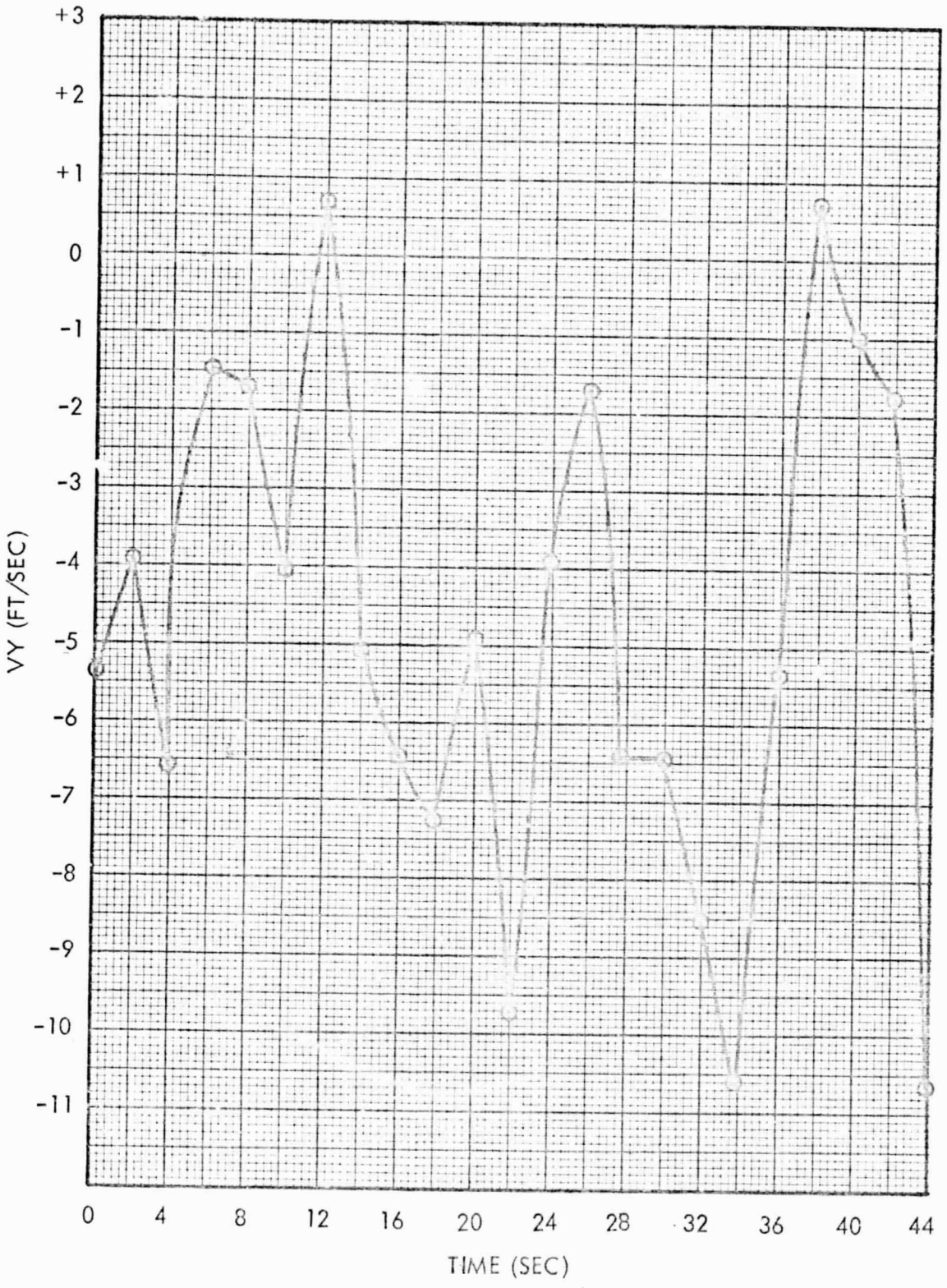


Figure 20. LR-73F, Pass 1, Landing Radar $V_y$ Component Velocity

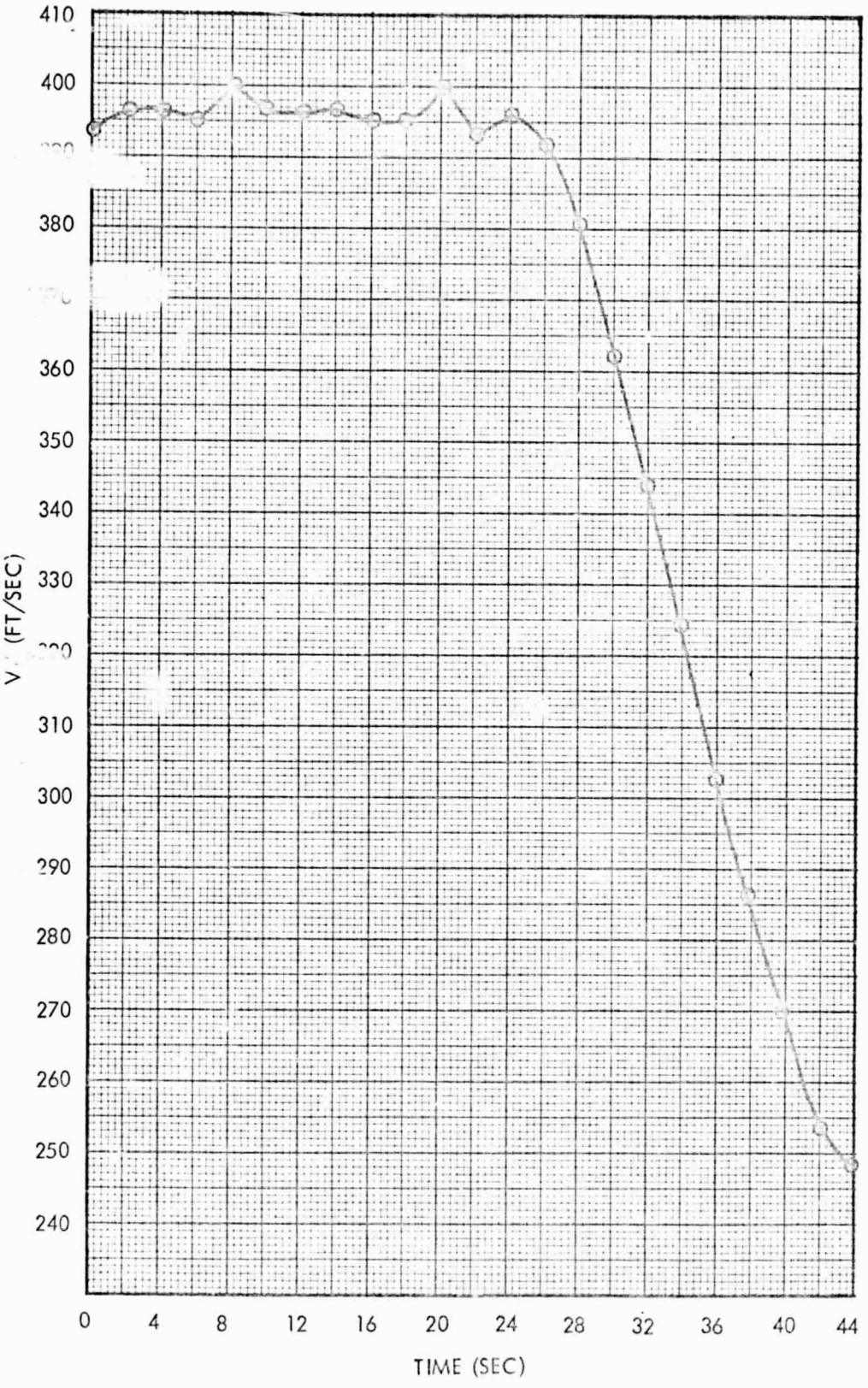


Figure 21. LR-73F, Pass 1, Landing Radar $V_z$ Component Velocity

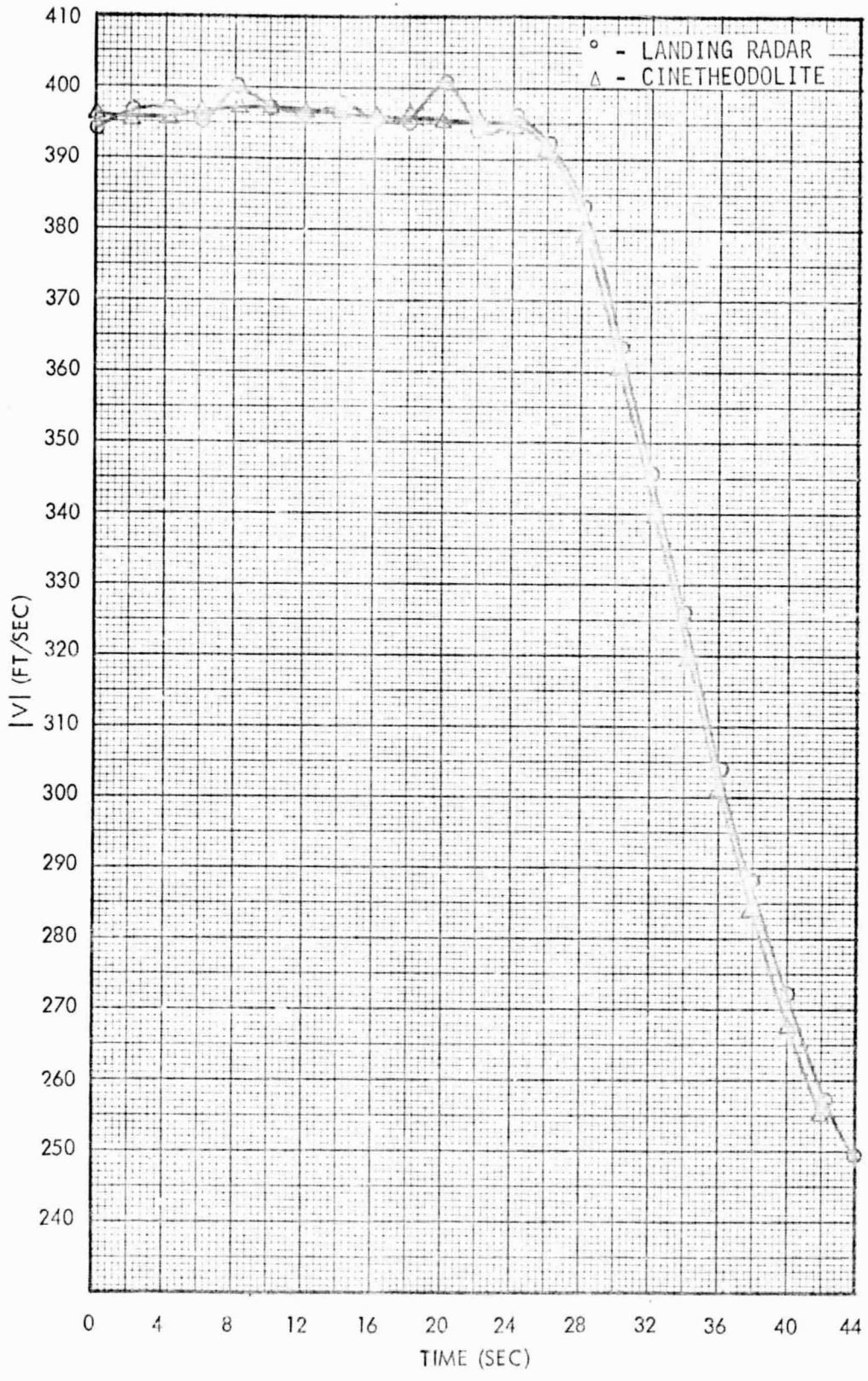


Figure 22. LR-73F, Pass 1, Landing Radar vs Cinetheodolite Vector Velocity

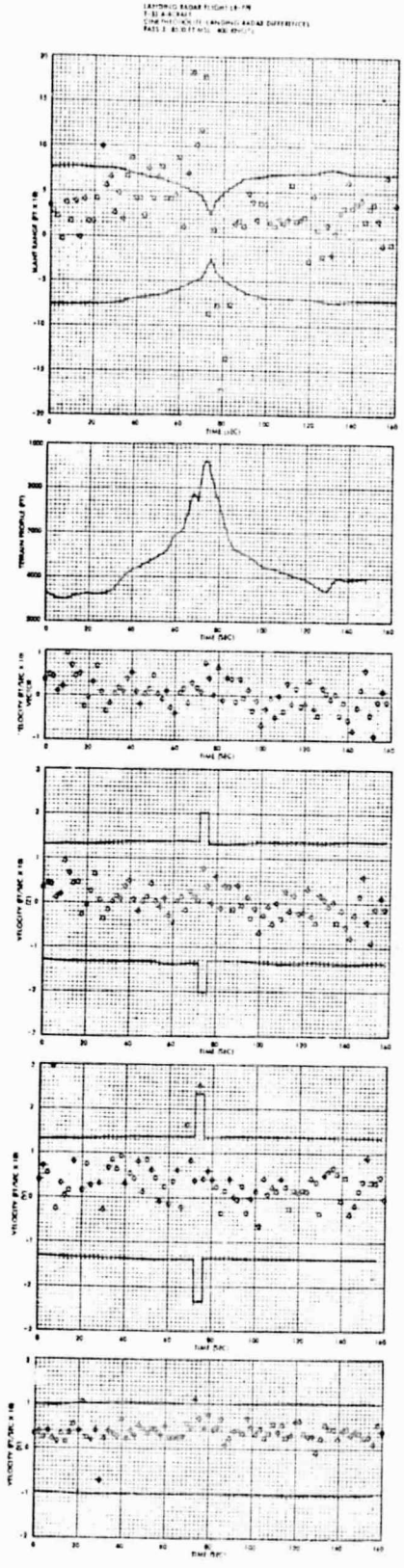

Figure 23. LR-77E, Pass 3, Cinetheodolite-Landing Radar Differences

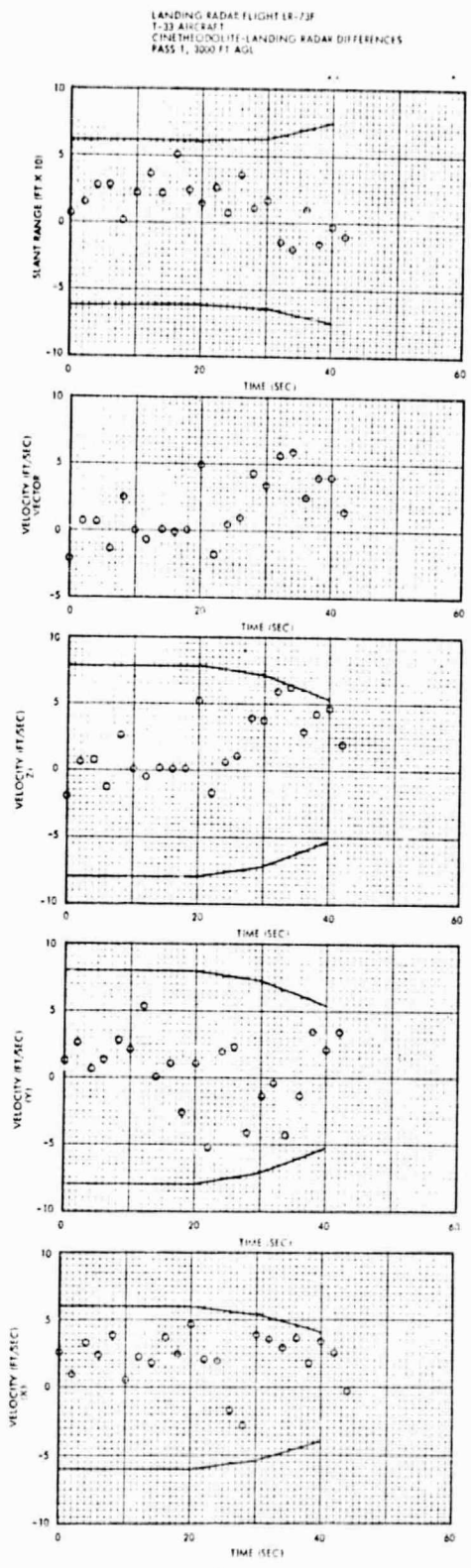


Figure 24. LR-73F, Pass 1, Cinetheodolite-Landing Radar Differences

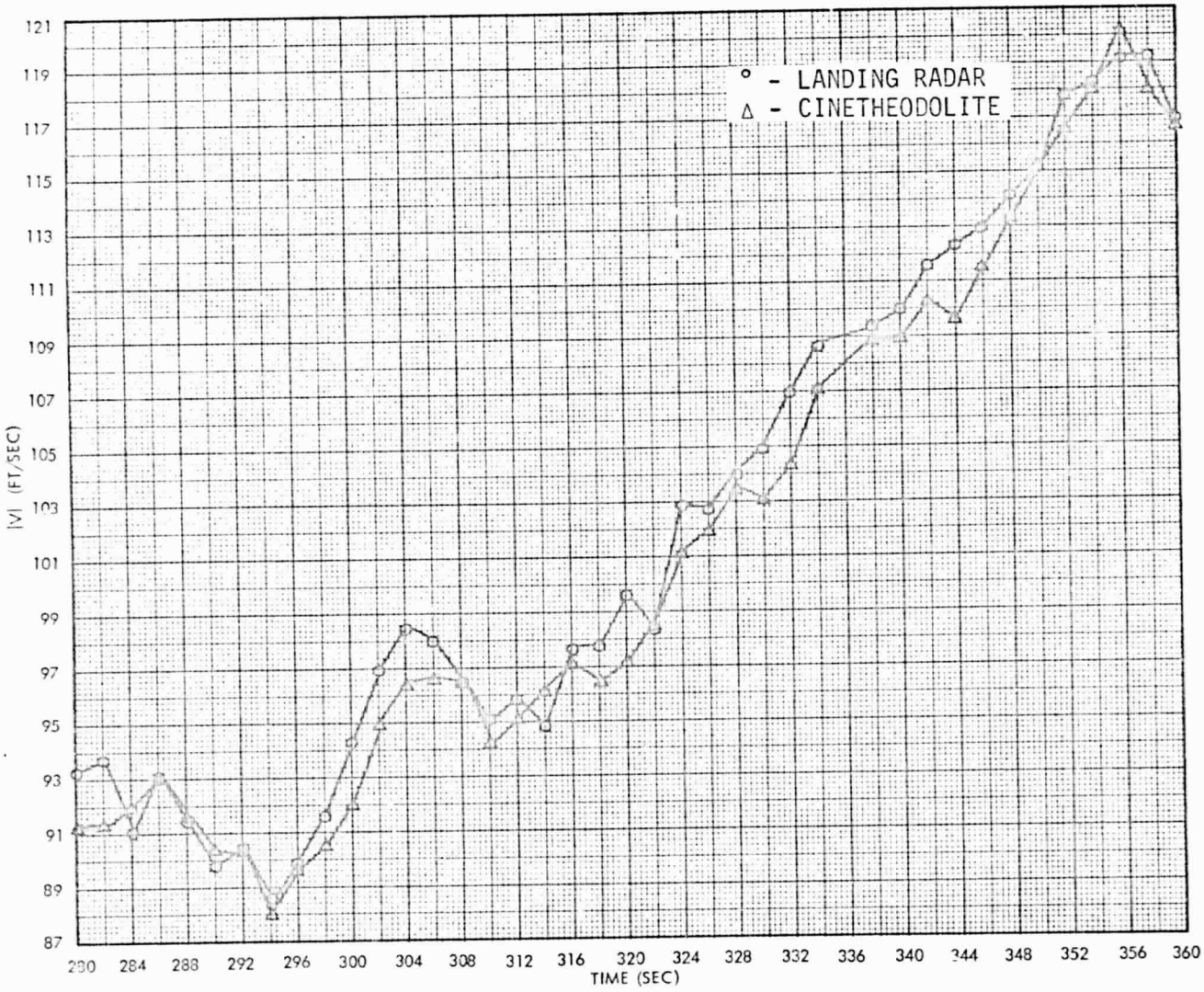


Figure 25. LR-58E, Pass 2 (Smoothest Portions), Radar vs Cinetheodolite Input for Vector Velocity Magnitude

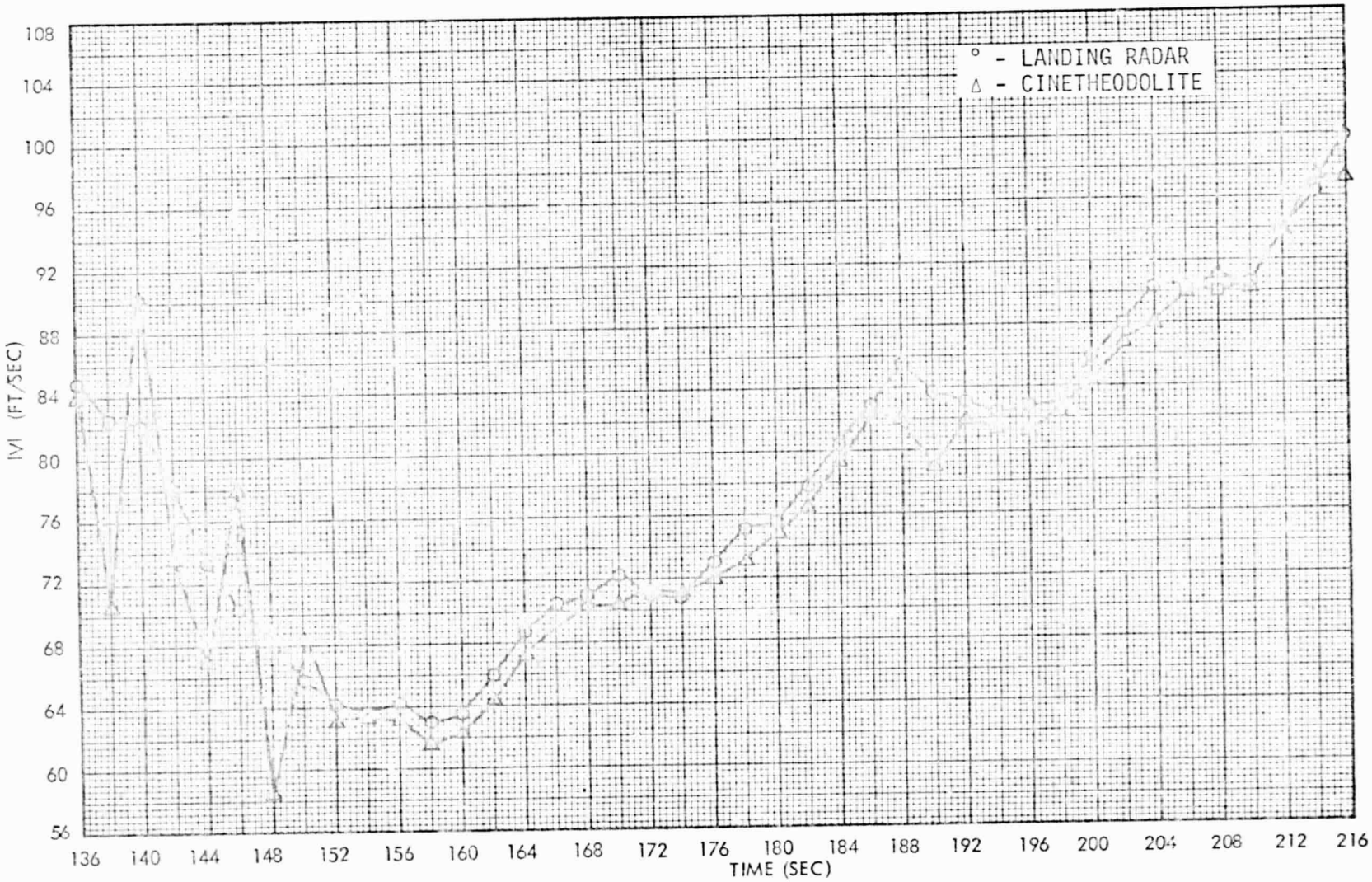


Figure 26. LR-58E, Pass 2 (Roughest Portions), Radar vs Cinetheodolite Input for Vector Velocity Magnitude

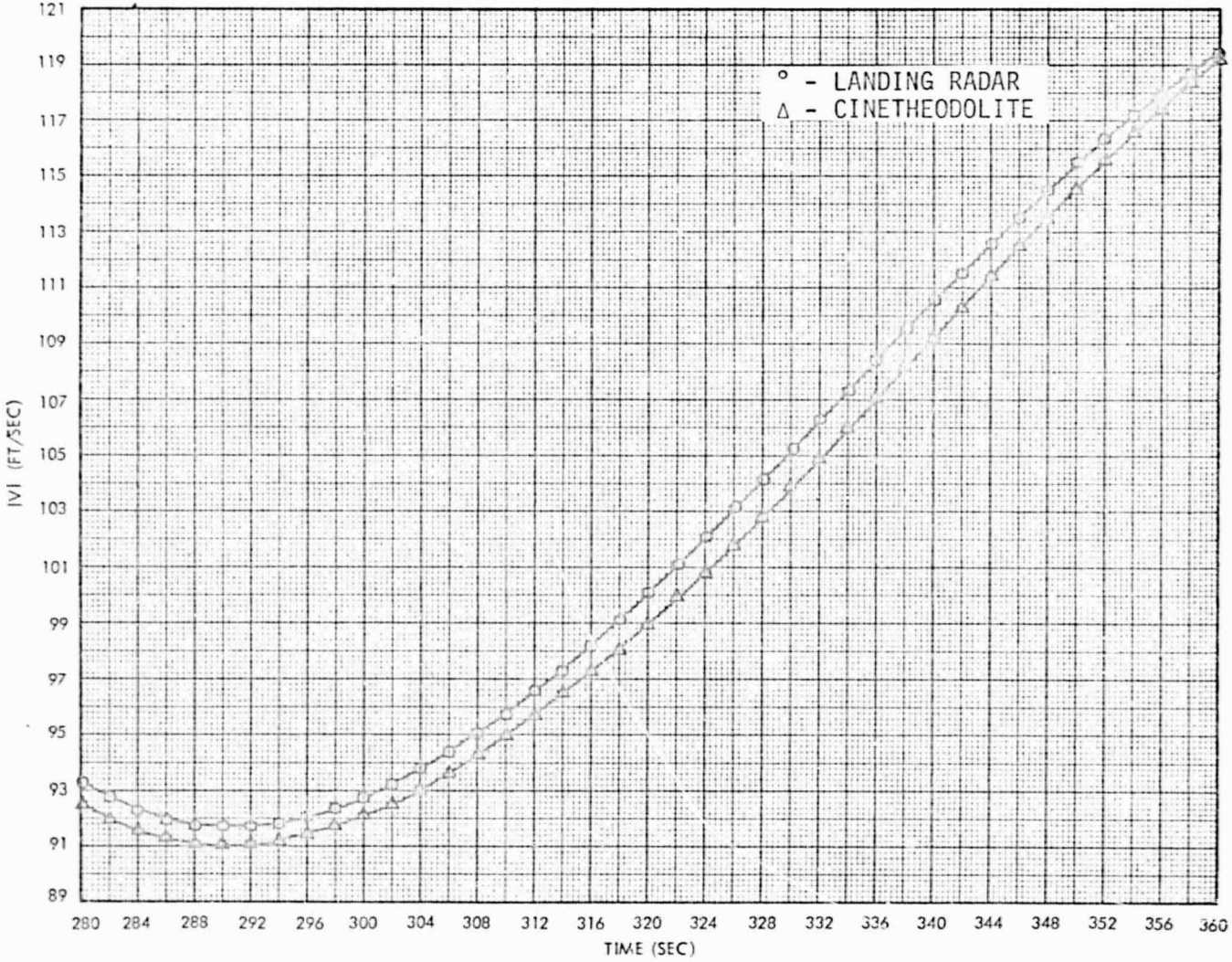


Figure 27. LR-58E, Pass 2 (Smoothest Portions), Third-degree Radar vs Cinetheodolite Polynomial for Vector Velocity Magnitude

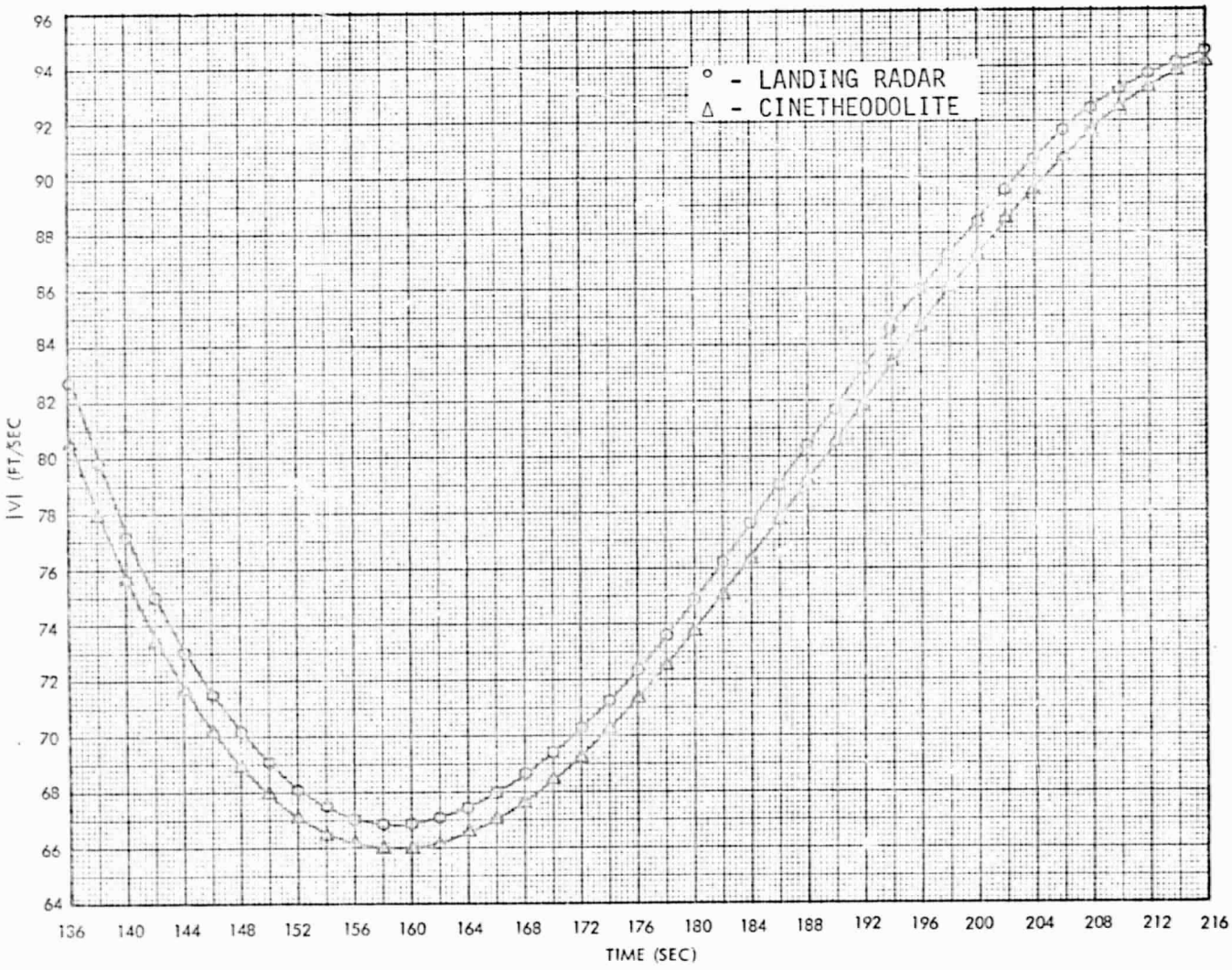


Figure 28. LR-58E, Pass 2 (Roughest Portions), Third-degree Radar vs Cinetheodolite Polynomial for Vector Velocity Magnitude

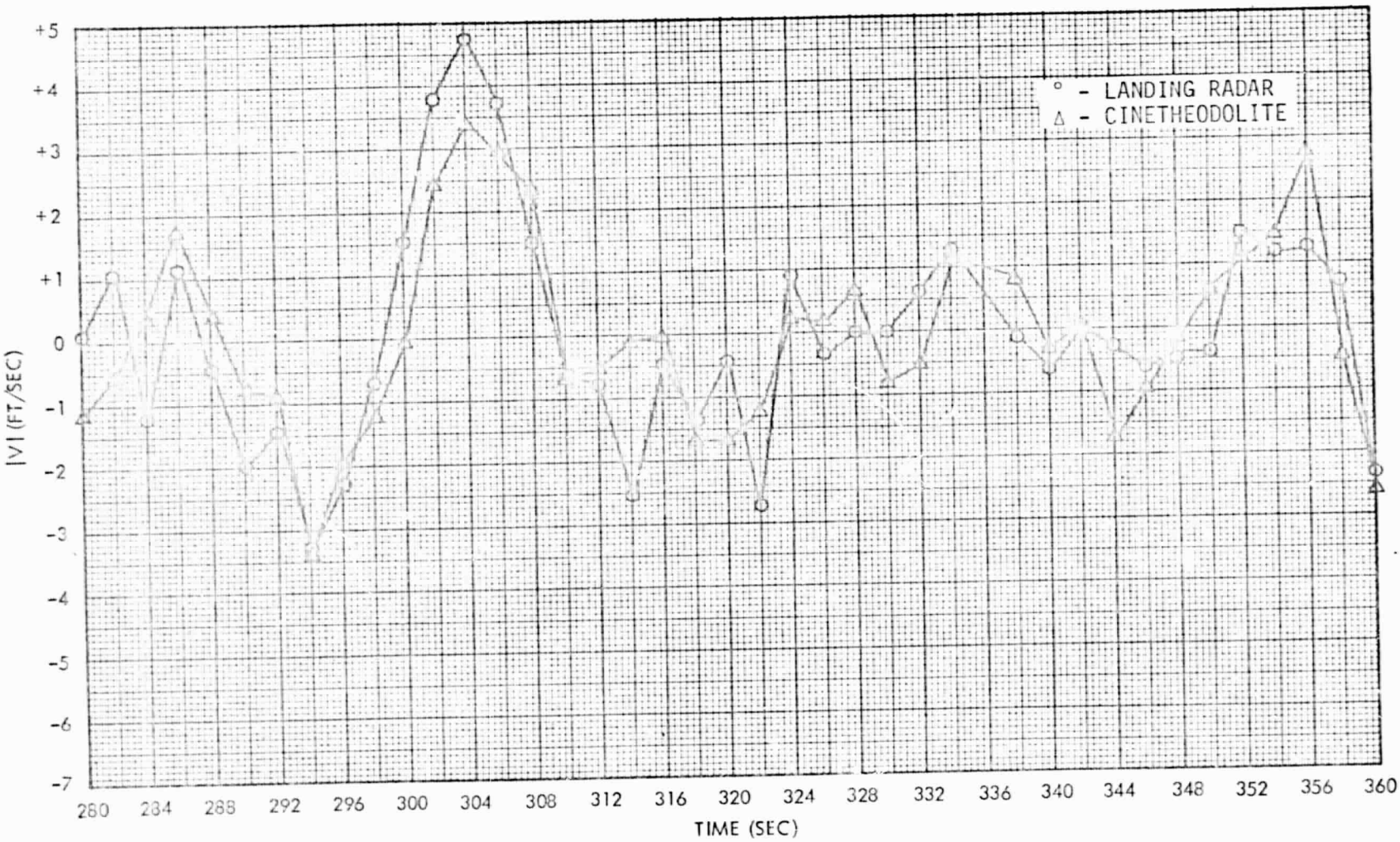


Figure 29. LR-58E, Pass 2 (Smoothest Portions), Third-degree Radar vs Cinetheodolite Residuals for Vector Velocity Magnitude

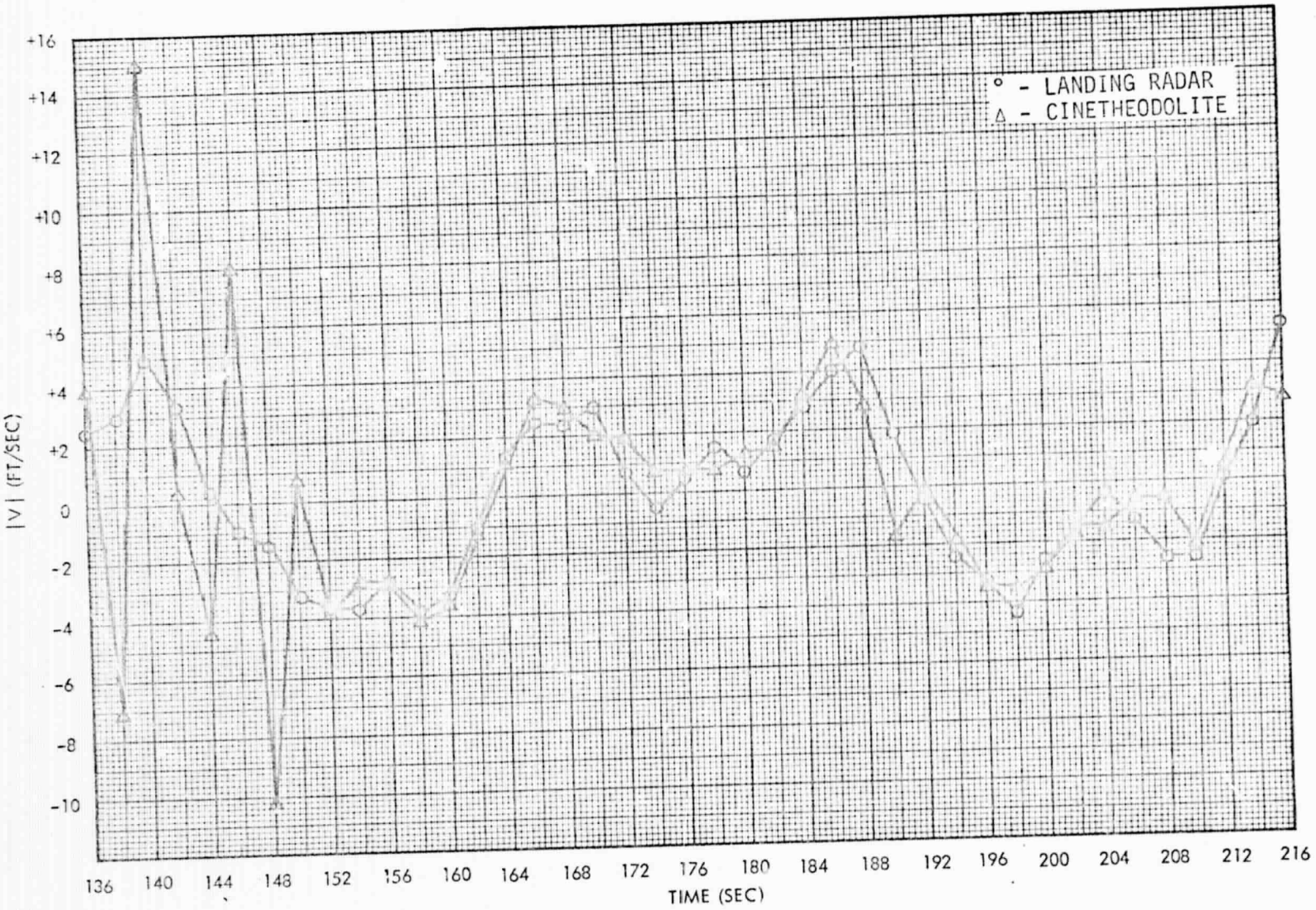


Figure 30. LR-58E, Pass 2 (Roughest Portions), Third-degree Radar vs Cinetheodolite Residuals for Vector Velocity Magnitude

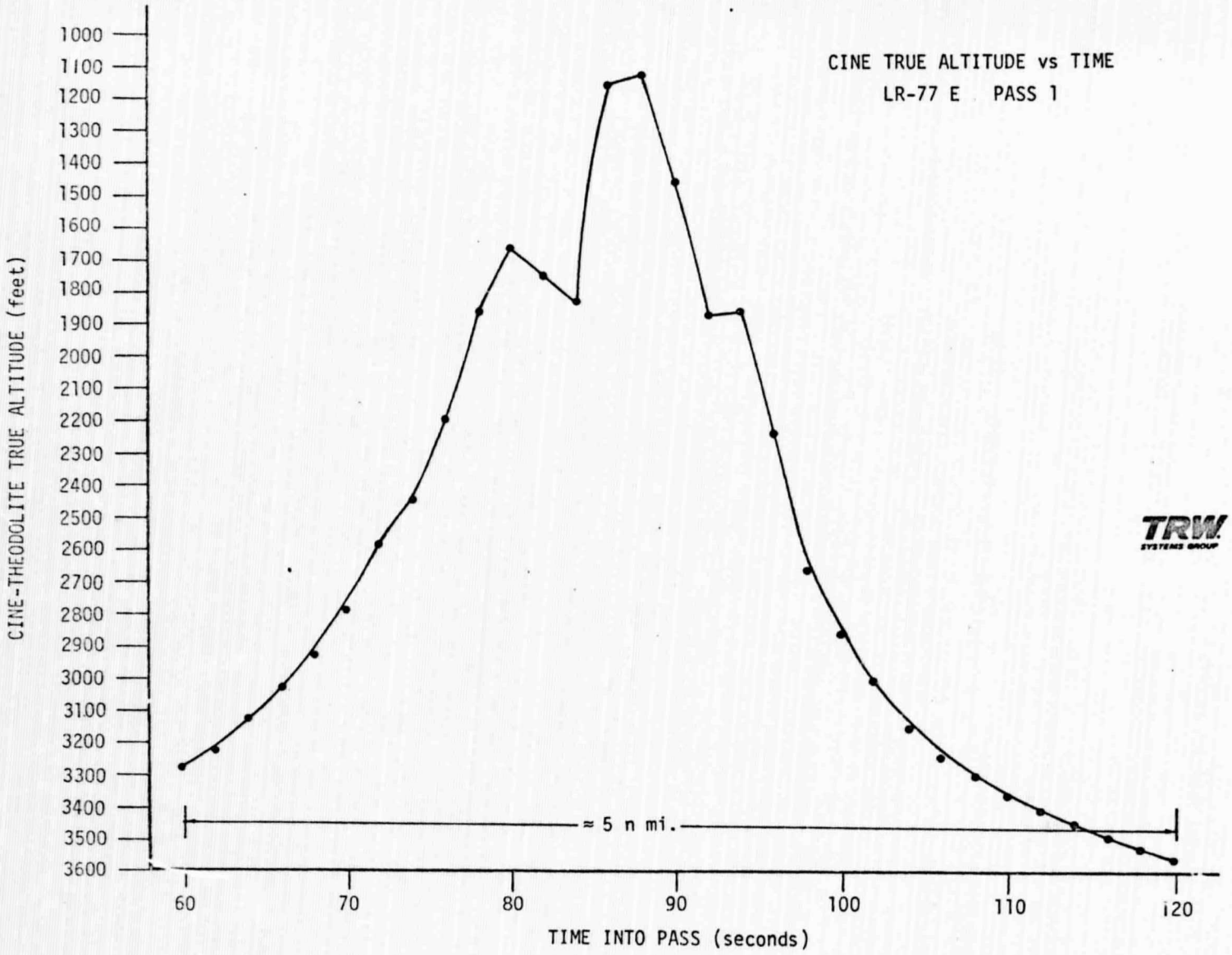


Figure 31. Reconstruction of Little Burro Peak Profile from Cinetheodolite True Altitude

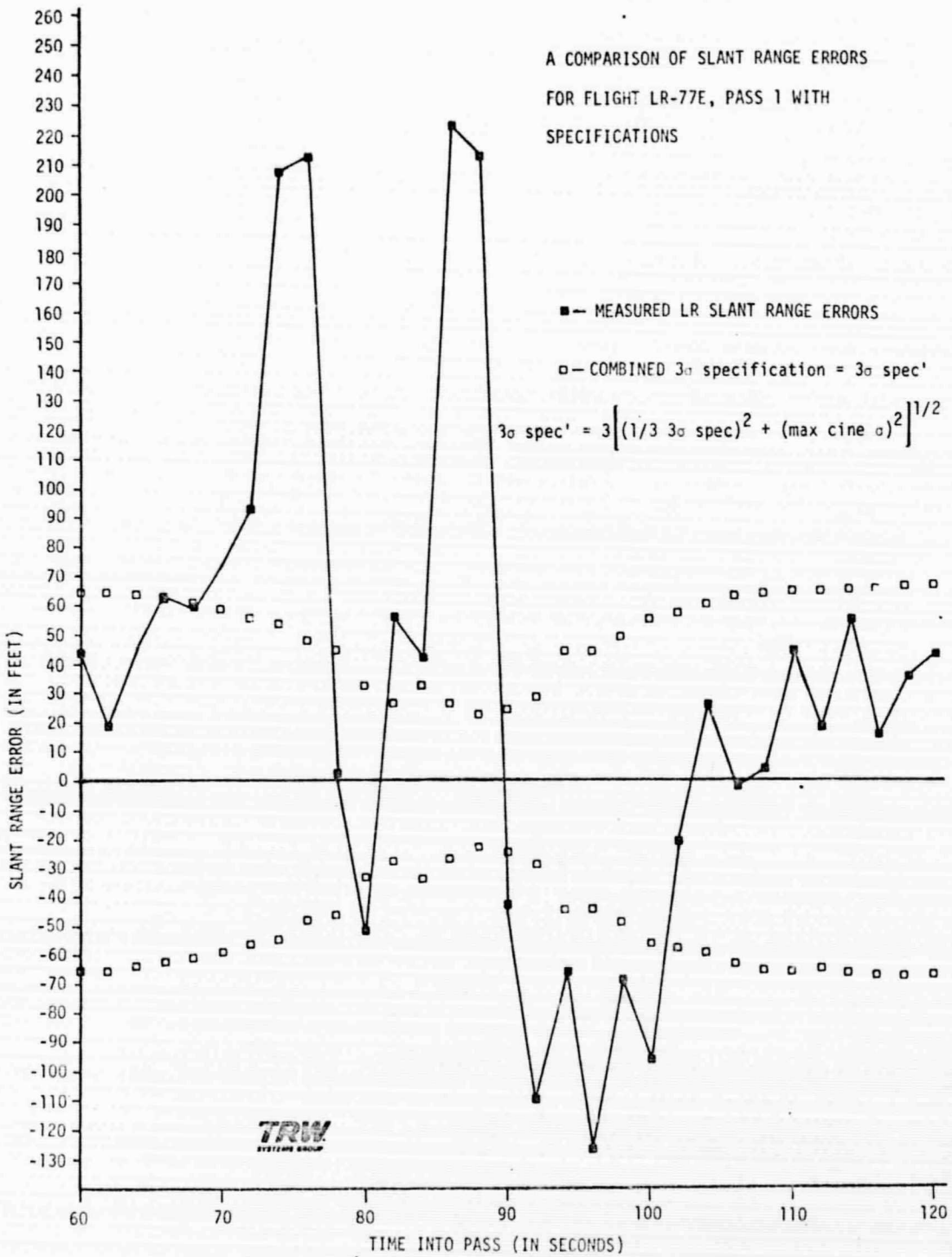


Figure 32. Comparison of Slant Range Errors (LR-Cine Residuals) with Specifications for Flight LR-77E, Pass 1

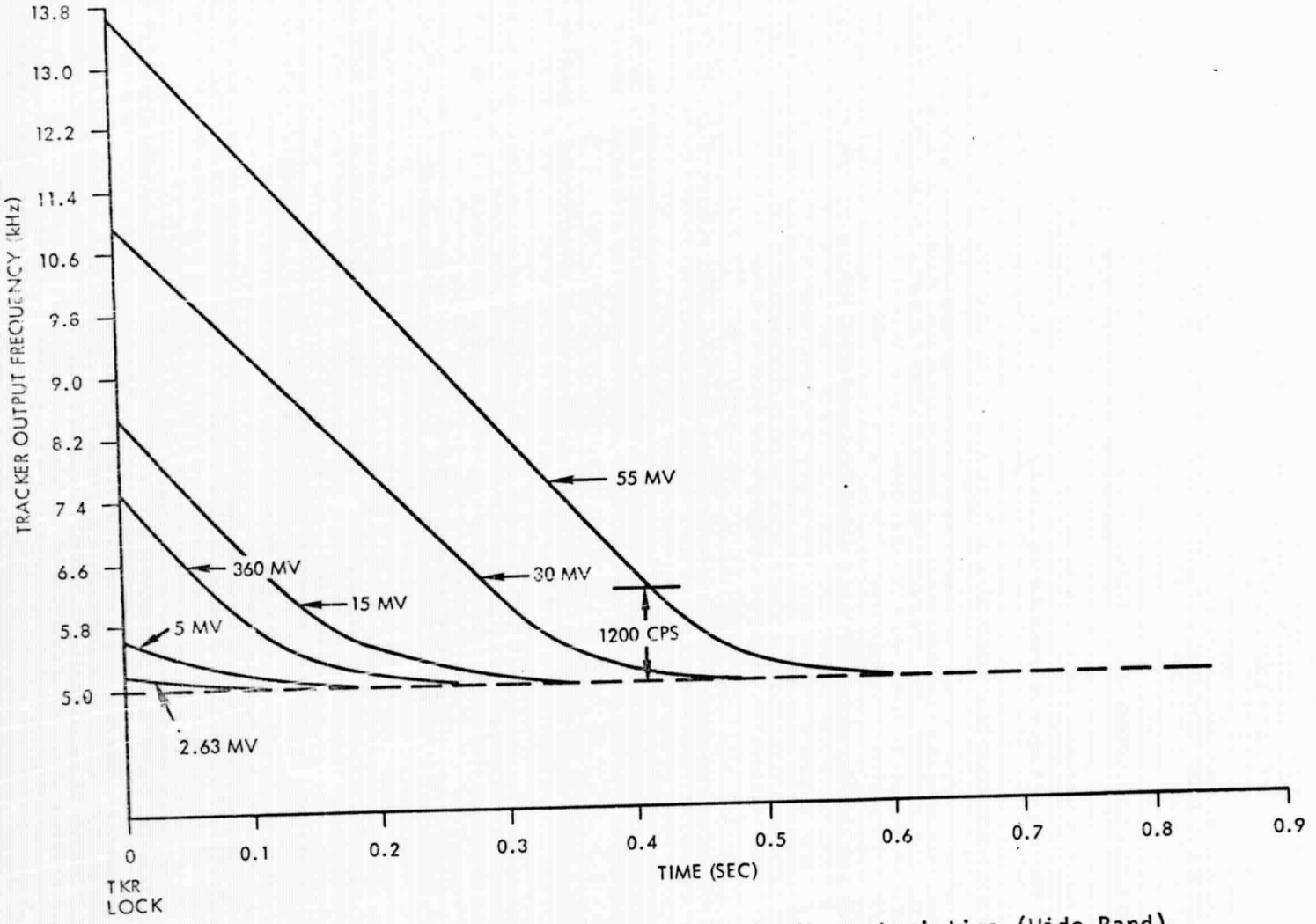


Figure 33. LR Frequency Tracker Pull-in Characteristics (Wide Band)

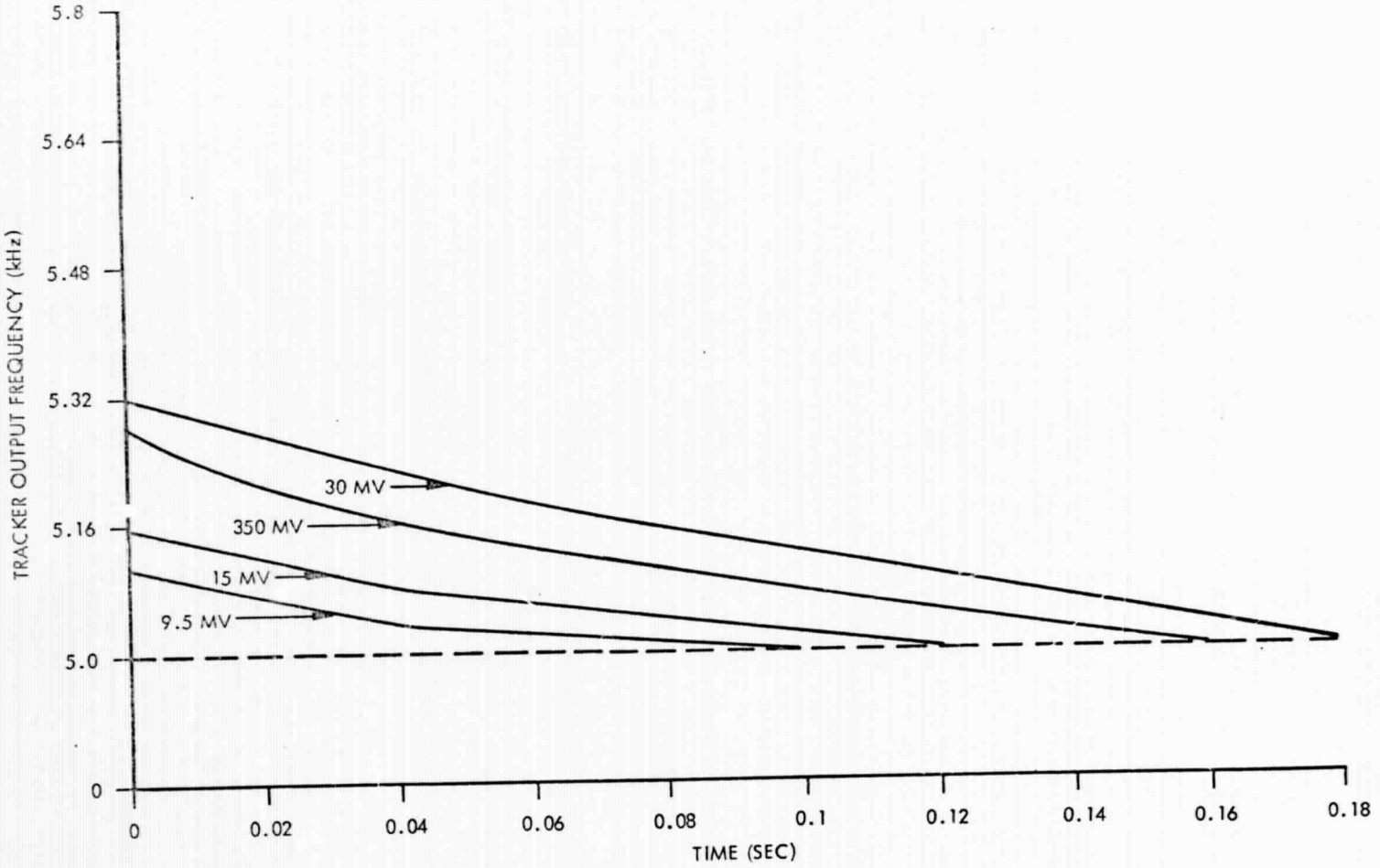


Figure 34. LR Frequency Tracker Pull-in Characteristics (Narrow Band)

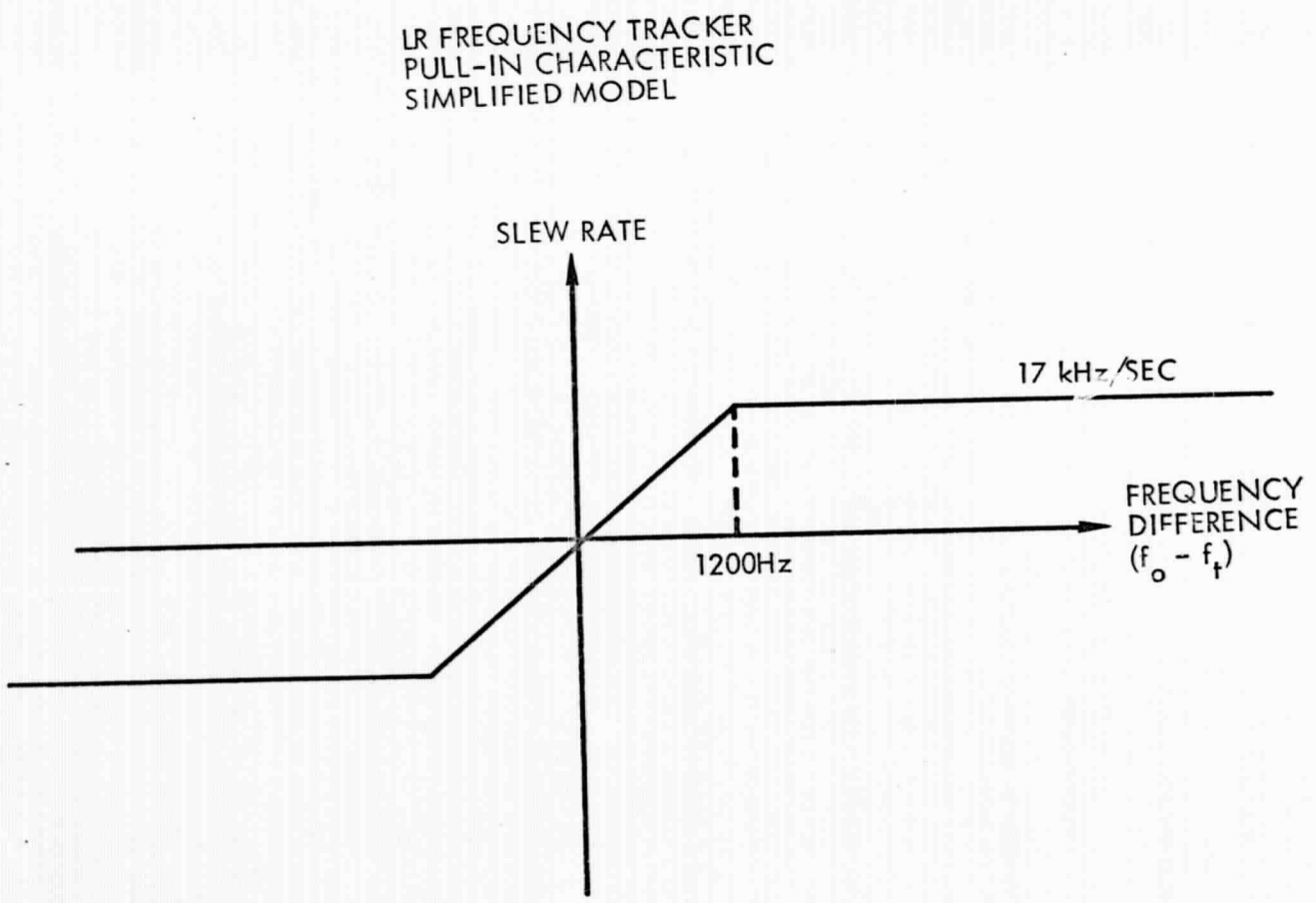


Figure 35. LR Frequency Discriminator-Filter-Loop Charateristic Estimate from Measured Data

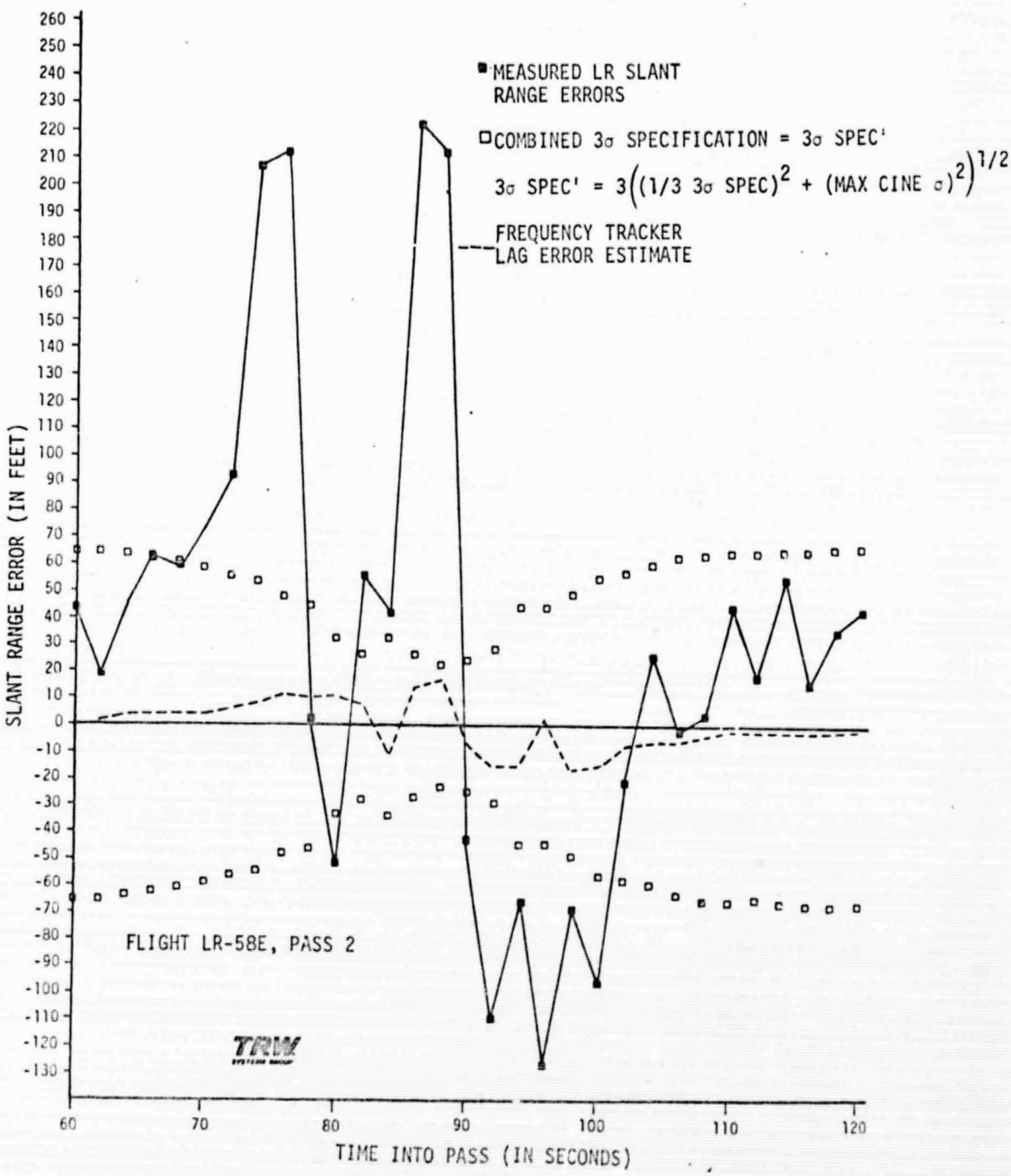


Figure 36. LR-Cine Residuals Compared to Tracker Lag Error Estimate (T-33)

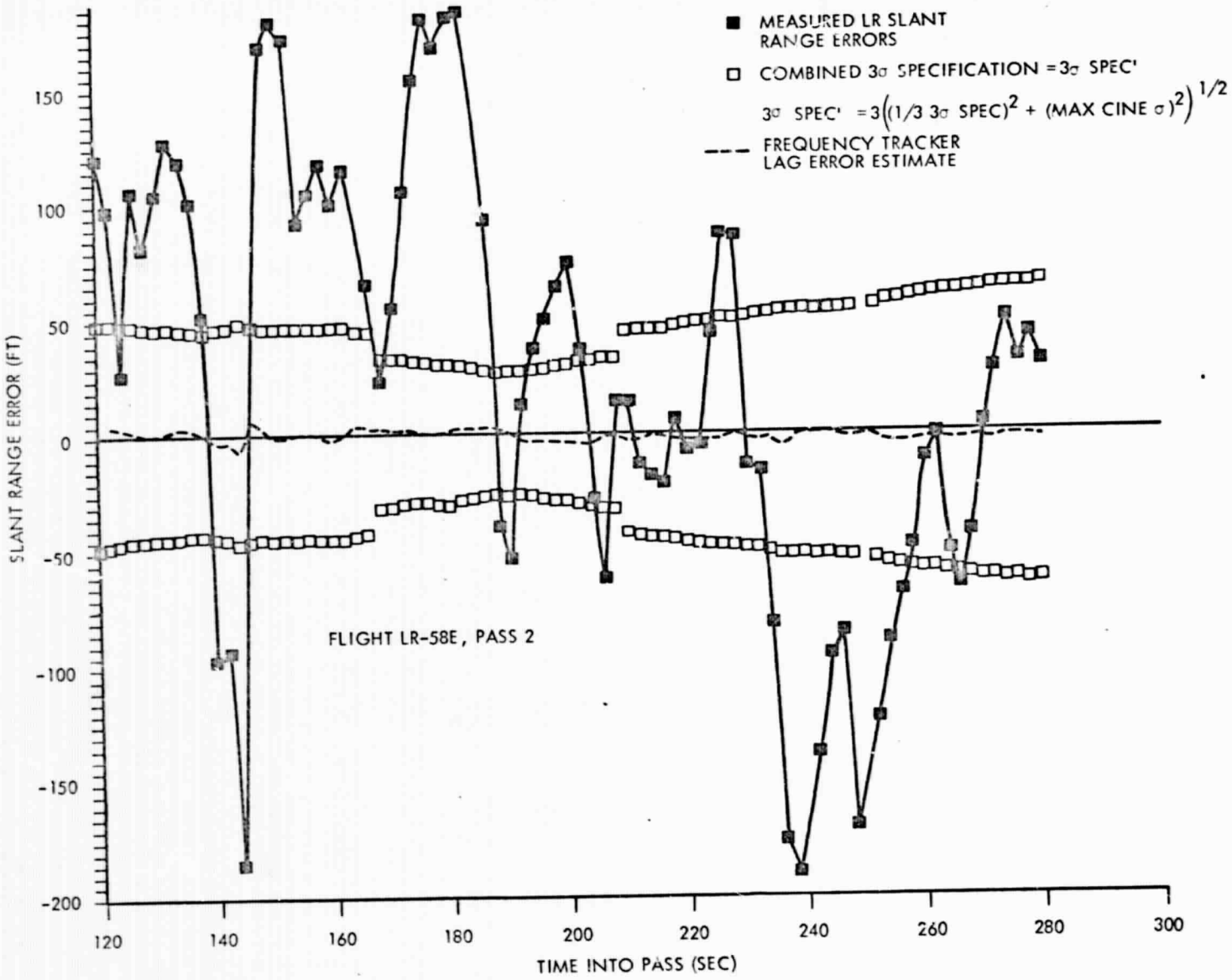


Figure 37. LR-Cine Residuals Compared to Tracker Lag Error Estimate (SH-3A)

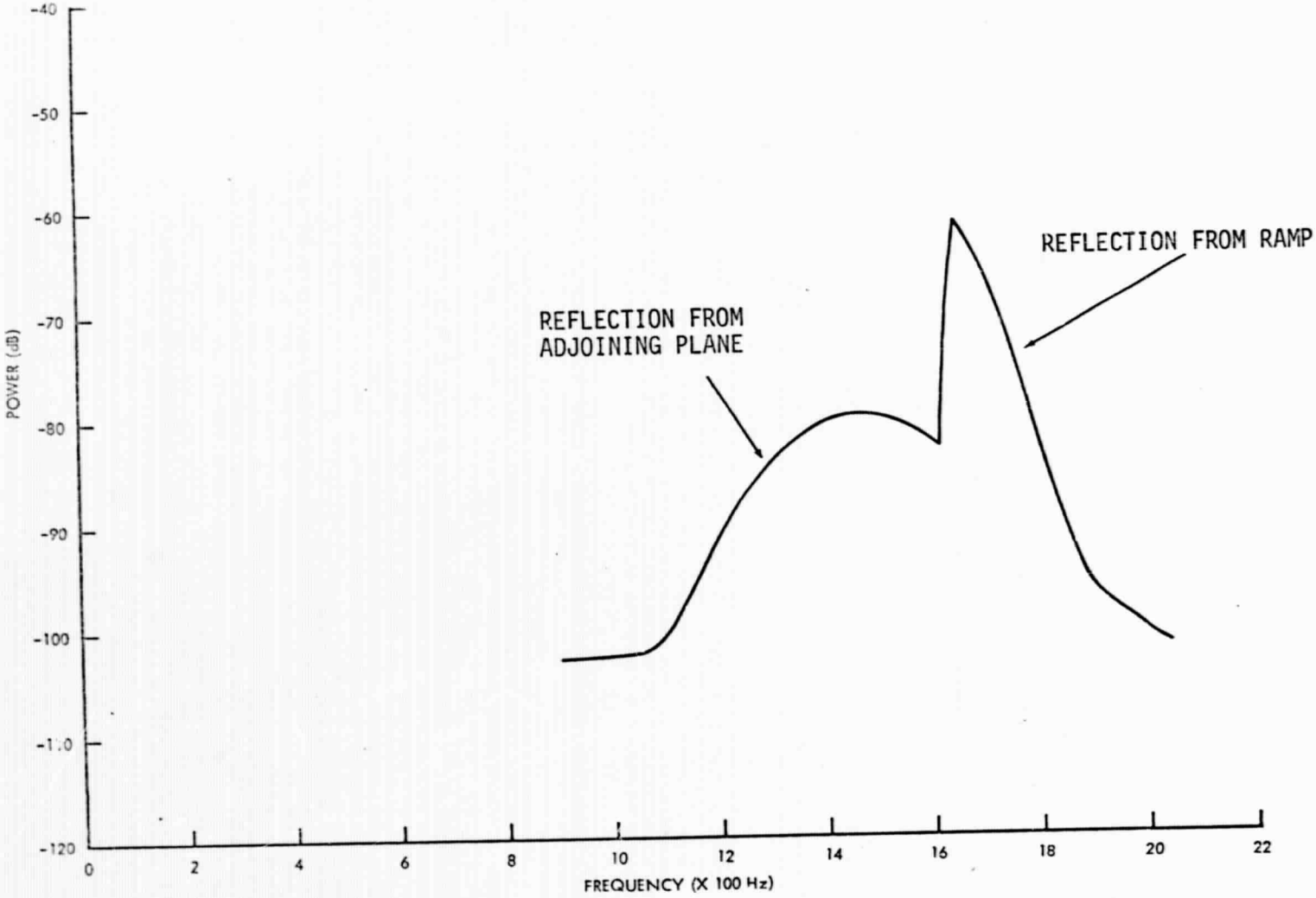


Figure 38. Sample Calculated Doppler Return Power Spectrum

## REFERENCES


1. Prepared by Computing and Software, Inc., Modified Program PEARL Project, Test LR-58E, Range ID 905/248/1, 12 December 1968.

2. Prepared by Computing and Software, Inc., Modified Program PEARL Project, Test LR-77E, Range ID 905/326/1, 15 January 1969.

3. Prepared by Computing and Software, Inc., Modified Program PEARL Project, Test LR-60J, Range ID 905/254/1, 12 December 1968.

4. Prepared by Computing and Software, Inc., Modified Program PEARL Project, Test LR-73F, Range ID 905/312/1, 14 January 1969.

5. LSP-470-2D, Master End-Item Specification for Lunar Module, 1 November 1968.

6. A. M. Matschke, "Error Analysis of the Rendezvous Radar Range, Range Rate, Shaft and Trunnion Functions - Final Report," TRW Report 11176-H301-RO-00, 24 July 1969.

7. L. K. Ridge, "Rendezvous Radar Data Analysis Final Report G-Mission," TRW Report 11176-H350-RO-00, 22 September 1969.

8. Prepared by Computing and Software, Inc., Modified Program PEARL Project, Test LR-74E, Range ID 905/313/1," 22 January 1969.

9. Published by Ryan Aeronautical, LM Landing Radar Technical Meeting, 10 April 1968.

10. D. E. Chambers, "A Comparison of the Computed LR Received Signal Spectrum and the 1967 PEARL Data," TRW Report 11176-H077-RO-00, 26 November 1968.

11. W. B. Warren and L. Armijo, A Technique for Computing Terrain Effects on Radar Return, TRW Project Technical Report, Task E-34C-1, 05952-H503-RO-00, 14 May 1968.